

# Theory of *ac* magnetoelectric transport in normal-metal – magnetic-insulator heterostructures

Oliver Franke, Duje Akrap, Ulli Gems, David A. Reiss, and Piet W. Brouwer  
*Dahlem Center for Complex Quantum Systems and Physics Department,  
 Freie Universität Berlin, Arnimallee 14, 14195 Berlin, Germany*

Electron-magnon coupling at the interface between a normal metal and a magnetically ordered insulator modifies the electrical conductivity of the normal metal, an effect known as spin-Hall magnetoresistance. It can also facilitate magnon-mediated current drag, the nonlocal electric current response of two normal metal layers separated by a magnetic insulator. In this article, we present a theory of these two spintronic effects and their nonlinear counterparts for time-dependent applied electric fields  $E(\omega)$ , with driving frequencies  $\omega$  up to the THz regime. We compare various mechanisms leading to a quadratic-in- $E$  response — Joule heating, spin-torque diode effect, and magnonic unidirectional spin-Hall magnetoresistance — and show how these can be disentangled by their characteristic dependences on  $\omega$  and the magnetization direction.

## I. INTRODUCTION

In spintronic devices containing magnetic insulators a central role is played by the conversion between magnonic and electronic spin and heat currents at magnetic-insulator–normal-metal interfaces. Such conversion is at the heart of the spin-Seebeck effect [1, 2], the excitation of a spin current in a normal metal by a temperature gradient across the interface. When combined with spin-charge conversion in the normal metal, which originates from the spin-Hall effect and its inverse [3, 4], the interfacial magnon-electron coupling also enables key spintronic effects, such as current-induced magnetization switching [5, 6], the spin-Hall magnetoresistance [7–17] or magnon-mediated current drag [18–26].

At the fundamental level, the coupling between magnonic and electronic spin and heat currents at the interface between a magnetic insulator and a normal metal has its origin in the spin-transfer torque [27, 28] and spin pumping [29]. For both effects, the strength of the coupling across the interface is described by the spin-mixing conductance [30]. Whereas the spin-transfer torque and spin pumping were originally discussed in the context of coherent magnetization motion, they are now understood to also govern the coupling of incoherent thermal magnons to electronic excitations in the normal metal [31, 32]. Upon combining the theoretical description of coupled spin and heat transport at the interface with semi-phenomenological theories for spin, charge, and heat transport in normal metals and magnetic insulators, a consistent theoretical framework arises for the description of a wide range of spintronic and spin-caloritronic effects in realistic spintronic devices containing magnetic insulators [15–19, 33–35].

With the availability of experimental methods to investigate spintronic effects in the high-frequency THz regime [36, 37], it becomes necessary to also theoretically describe such effects in the limit of ultrafast driving. In this article, we accomplish this task for the prototypical geometry of an N|F|N trilayer (N: normal metal, F: ferromagnetic insulator), shown schematically in Fig. 1.

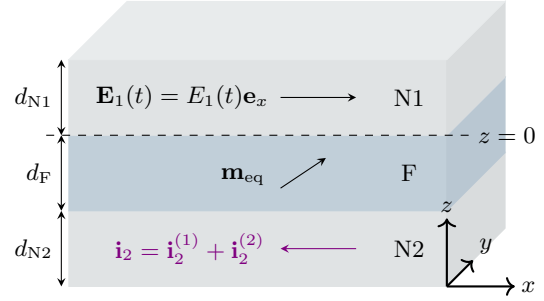


FIG. 1. Geometry of the N|F|N trilayer consisting of two normal metals N1 and N2 and a magnetically ordered insulator F. An in-plane electric field  $\mathbf{E}_i(t) = E_i(t)\mathbf{e}_x$  in one of the normal-metal layers gives rise to charge currents  $\mathbf{i}_j = \mathbf{i}_j^{(1)} + \mathbf{i}_j^{(2)}$  in both layers. In this article, we calculate the charge currents  $\mathbf{i}_j^{(1)}$  linear in  $E_i$  as well as the charge currents  $\mathbf{i}_j^{(2)}$  quadratic in the applied field  $E_i$  for driving fields  $E_i(t) \propto \cos(\omega t)$  with driving frequencies ranging from the *dc* limit  $\omega = 0$  to the THz regime.

Specifically, we consider charge currents  $\mathbf{i}_1$  and  $\mathbf{i}_2$  in both normal-metal layers to linear and quadratic order in the electric field  $\mathbf{E}_1(\omega)$  in one of the layers. Spintronic effects captured in this setting are the spin-Hall magnetoresistance, which describes the dependence of the linear conductivity of the normal-metal layers on the orientation of the magnetization in F, the magnon current drag, which is the flow of an electrical current as a result of an applied electric field in the other layer, as well as nonlinear versions of these effects, such as the unidirectional spin-Hall magnetoresistance [38–40] or spin-torque diode effect [41–47]. Our article builds on existing theories of these effects in the *dc* limit [15–19, 34, 48–51] and extends them to the regime of high driving frequencies  $\omega$ . It also extends previous work on linear charge transport in F|N bilayers with *ac* driving by Kampfrath and two of the authors [52].

To understand the frequency dependence of the spintronic response of an N|F|N trilayer, a theoretical description of the whole system, rather than of its separate com-

ponents, is essential. That spintronic effects in an N|F|N trilayer at finite driving frequency  $\omega$  differ from those in the *dc* limit has its origin in the frequency dependence of magnon transport through the magnetic insulator F [52]. For incoherent magnons, relevant time scales are the various elastic and inelastic relaxation times and the time required to diffuse across F [34, 35]. For coherent magnons, the relevant time scale is the time-of-flight between the two F|N interfaces. For YIG, these time scales result in characteristic frequencies in the THz range and below, depending on device parameters. On the other hand, the fundamental processes coupling spin and charge currents at the individual F|N interfaces, as well as the spin-charge conversion in N mediated by the spin-Hall effect and its inverse, may be considered frequency-independent, at least for frequencies up to the THz range. The reason is that, unless the interface is very disordered, the transit time of electrons and magnons through the interface region is simply too short to result in an appreciable frequency dependence. Indeed, the spin-transfer torque [53, 54], the interfacial spin-Seebeck effect [55, 56], and the spin-Hall effect and its inverse [57, 58] have been shown to persist unchanged well into the THz frequency range.

Spin transport across the magnetic insulator F has contributions from coherent and from incoherent (thermal) magnons. Which of these contributions dominates the response depends on the driving frequency  $\omega$ . As a rule of thumb, coherent magnetization dynamics are relevant for spin-Hall magnetoresistance at low frequencies for thin F layers [15, 16] (although there also is a smaller contribution from thermal magnons [17]) and at high frequencies near magnon resonances [59, 60], whereas incoherent magnons dominate the response otherwise [52]. The nonlocal response, *i.e.*, magnon-mediated electric current drag, is mediated by incoherent magnons at low frequencies [18, 19], whereas coherent magnons are relevant at resonances only. A theory that describes spintronic effects for frequencies ranging from zero to the THz regime must therefore address spin transport by coherent and incoherent magnons on equal footing. We here accomplish this by using an effective description in terms of “spin impedances” [52], whereby coherent and incoherent magnons constitute parallel channels of spin transport through F.

Our theory not only considers the local and nonlocal current response linear in electric field  $\mathbf{E}$  applied to one of the normal-metal layers, but also the nonlinear response quadratic in  $E$ . For a driving field at finite frequency  $\omega$ , the quadratic response takes place at zero frequency and at frequency  $2\omega$ . The quadratic-in- $E$  response close to zero driving frequency is known as the “unidirectional spin-Hall magnetoresistance” [38, 39, 49]. It was originally observed in multilayers involving a metallic ferromagnet, but subsequently predicted [50, 51] and observed [40] in bilayers featuring a ferromagnetic insulator F. Since electronic heat current is quadratic in  $E$ , an important source of nonlinear response of the N|F|N trilayer

is the linear coupling between spin and heat currents at the F|N interfaces [21].

For driving frequencies that allow for the resonant excitation of coherent magnon modes in F, an additional source of nonlinear response is the spin-torque diode effect [41, 42], the large-amplitude magnetization precession associated with that magnon mode [43–48]. We find that, depending on the driving frequency  $\omega$ , both these sources of nonlinear response can dominate the charge current response. To complete our theoretical analysis, we also consider a third source of nonlinear current response, which is rooted in the nonlinearity of the interfacial coupling [51].

The remainder of this article is organized as follows: In Sec. II, we introduce the system of interest and establish the required notation. In Sec. III, we calculate and discuss the local and nonlocal linear conductivities. The quadratic current response is considered in Sec. IV. In Secs. III and IV we present our final results in the form of dimensionless conductivity corrections, which allows for an easy comparison of different effects and estimates of their magnitude. We conclude with a discussion of our results in Sec. V. Our findings are illustrated by a numerical evaluation of local and nonlocal conductivities for a Pt|YIG|Pt trilayer. To facilitate the evaluation of our results for device parameters not considered by us or for other material combinations, an open source code is available to evaluate local and nonlocal, linear and nonlinear response for different materials and system sizes [61].

## II. TRILAYER SYSTEM AND NOTATION

The N|F|N trilayer we consider is shown schematically in Fig. 1. It consists of two normal metals N1 and N2, separated by a ferromagnetic insulator F. We choose coordinates such that N1 and N2 are located at  $0 < z < d_{N1}$  and  $-d_F - d_{N2} < z < -d_F$ , whereas the ferromagnetic insulator F is at  $-d_F < z < 0$ .

Spatially uniform time-dependent electric fields

$$E_i(t) = E_i(t), \quad i = 1, 2, \quad (1)$$

are applied in N1 and N2 in the  $x$ -direction, where

$$E_i(t) = \frac{1}{2\pi} \int_{-\infty}^{+\infty} d\omega E_i(\omega) e^{-i\omega t}. \quad (2)$$

In response to the applied electric fields, charge current densities  $i_j^{x,y}(z, t)$ ,  $j = 1, 2$ , flow in the two normal-metal layers. The goal of our calculation is to find the spatially averaged current densities for each of the normal-metal layers to linear and quadratic order in the applied fields,

$$\bar{i}_j^{x,y}(t) = \bar{i}_j^{x,y}(t)^{(1)} + \bar{i}_j^{x,y}(t)^{(2)}. \quad (3)$$

The current response with  $j = i$  is local, whereas the response with  $j \neq i$  is nonlocal.

In addition to the in-plane charge current density  $i^{x,y}(z,t)$ , the relevant variables for the charge and spin currents in the normal metals N1 and N2 are the out-of-plane spin current density  $\mathbf{i}_s(z,t)$ , and the spin accumulation  $\mathbf{e}\mathbf{u}_s(z,t)$ . (We here omit the subscript  $j$  labeling the normal metal layer Nj to keep the notation simple.) The position argument is  $0 < z < d_N$  for N1 and  $-d_F - d_{N2} < z < -d_F$  for N2. Here, and in the following, we denote spatial directions by superscripts and spin directions by subscripts or boldface vector notation. In the normal metals, the spin current density is defined as  $i_{sz}^z = i_{\uparrow}^z - i_{\downarrow}^z$ , whereas the charge current density  $i^z = i_{\uparrow}^z + i_{\downarrow}^z$  is separated into spin up and spin down parts with respect to the  $z$ -axis. Similarly, the spin accumulation is defined as  $e\mathbf{u}_{sz} = \mu_{\uparrow} - \mu_{\downarrow}$ , where  $\mu_{\sigma}$  is the chemical potential for electrons of spin  $\sigma$ , the spin direction being defined with respect to the  $z$ -axis. To ensure that response relations for spin and charge have the same form, we have chosen units such that the spin current and spin accumulation have the dimension of an equivalent charge current and an equivalent voltage, respectively. Definitions for the  $x$  and  $y$  components of the spin current density and spin accumulation are analogous.

Since charge, spin, and heat transport are coupled in the N|F|N trilayer, we must also consider heat transport. For consistency, we also measure the heat current density  $i_Q$  in units of an equivalent charge current density,

$$i_Q^z(z,t) = \frac{2e}{k_B T} j_Q^z(z,t), \quad (4)$$

where  $j_Q^z$  is the heat current in units of [energy density  $\times$  velocity]. We also introduce the corresponding equivalent voltage for a deviation  $\Delta T$  of the temperature from its equilibrium value,

$$u_Q(z,t) = \frac{k_B}{e} \Delta T(z,t). \quad (5)$$

The (position dependent) magnetization direction of the ferromagnetic insulator F is denoted by the unit vector  $\mathbf{m}(z,t)$ , where  $-d_F < z < 0$ . The equilibrium magnetization direction is denoted

$$\mathbf{m}_{eq} = m_x \mathbf{e}_x + m_y \mathbf{e}_y + m_z \mathbf{e}_z. \quad (6)$$

We will find it useful to decompose vector-valued variables, such as the magnetization direction  $\mathbf{m}(z,t)$ , the spin current  $\mathbf{i}_s(z,t)$ , or the spin accumulation  $\mathbf{e}\mathbf{u}_s(z,t)$  into components parallel to and perpendicular to  $\mathbf{m}_{eq}$ . Hereto, we choose a complex unit vector  $\mathbf{e}_{\perp}$ , whose real and imaginary parts span the perpendicular plane to  $\mathbf{m}_{eq}$  and that fulfills

$$\mathbf{e}_{\perp} \times \mathbf{m}_{eq} = i \mathbf{e}_{\perp}. \quad (7)$$

A convenient choice is [52]

$$\mathbf{e}_{\perp} = \frac{1}{\sqrt{2(m_x^2 + m_z^2)}} [(m_x^2 + m_z^2) \mathbf{e}_y - (m_z m_y - i m_x) \mathbf{e}_z - (m_x m_y + i m_z) \mathbf{e}_x]. \quad (8)$$

The decomposition into components parallel to and perpendicular to  $\mathbf{m}_{eq}$  then amounts to expressing all spin-related quantities in the basis  $\{\mathbf{m}_{eq}, \mathbf{e}_{\perp}, \mathbf{e}_{\perp}^*\}$ . In particular, the magnetization direction  $\mathbf{m}(z,t)$  reads

$$\mathbf{m}(z,t) = m_{\parallel}(z,t) \mathbf{m}_{eq} + m_{\perp}(z,t) \mathbf{e}_{\perp} + m_{\perp}^*(z,t) \mathbf{e}_{\perp}^*, \quad (9)$$

where  $m_{\parallel}(z,t) = \sqrt{1 - 2|m_{\perp}(z,t)|^2}$  because the vector  $\mathbf{m}(z,t)$  is normalized.

The Fourier transform of the observables defined here is the same as that of the electric field  $E(t)$ , see Eq. (2). Since  $E(t)$  is real, one has  $E(-\omega) = E^*(\omega)$ . The time-domain variables  $m_{\perp}(z,t)$ ,  $\mathbf{i}_{s\perp}(z,t)$ , and  $\mathbf{u}_{s\perp}(z,t)$  are complex, so that their Fourier transforms at frequencies  $\omega$  and  $-\omega$  are not complex conjugates of each other. Because the dynamical variables in N1, N2, and F are mainly needed at the ferromagnet-normal-metal interfaces at  $z = 0$  and  $z = -d_F$ , we use the short-hand notation  $\mathbf{u}_{s1}(t) = \mathbf{u}_s(0,t)$ ,  $\mathbf{u}_{s2}(t) = \mathbf{u}_s(-d_F,t)$  and analogously for the other variables. (The exception to this notation is the charge current density  $\bar{i}_j^{x,y}(t)$  of Eq. (3), which is the average over the cross section of the layers N1 or N2.)

### III. LINEAR RESPONSE

To linear order in the applied fields, the spatially averaged charge current densities  $\bar{i}_j^{x/y}(\omega)$ ,  $j = 1, 2$ , are related to the applied field  $E_i(\omega)$  via the conductivities  $\sigma_{ji}^{xx}(\omega)$  and  $\sigma_{ji}^{yx}(\omega)$ ,

$$\begin{aligned} \bar{i}_j^x(\omega)^{(1)} &= \sum_{i=1}^2 \sigma_{ji}^{xx}(\omega) E_i(\omega), \\ \bar{i}_j^y(\omega)^{(1)} &= \sum_{i=1}^2 \sigma_{ji}^{yx}(\omega) E_i(\omega). \end{aligned} \quad (10)$$

In this Section, we calculate the nonlocal conductivities  $\sigma_{ji}^{xx}(\omega)$  and  $\sigma_{ji}^{yx}(\omega)$ ,  $j \neq i$ , as well as corrections  $\delta\sigma_{ii}^{xx}(\omega)$  and  $\delta\sigma_{ii}^{yx}(\omega)$  to the local conductivities  $\sigma_{ii}^{xx}(\omega)$  and  $\sigma_{ii}^{yx}(\omega)$  that arise from the coupling with the ferromagnetic insulator F and, hence, depend on the magnetization direction  $\mathbf{m}_{eq}$ .

We first review the fundamental relations between charge, spin, and heat currents, electron and magnon temperatures, and spin accumulations to lowest order in the applied electric field. In Secs. III A, III B, and III C, we present separate relations for the bulk of the two normal-metal layers N1 and N2, across the F|N interfaces, and for the bulk of the ferromagnetic insulator F, respectively. Following Ref. 52, we find it advantageous to formulate these relations in terms of impedances, the coefficients of proportionality between spin or heat currents and (differences of) spin accumulations or temperatures, respectively. For the interior of N1, F, and N2, the derivation of these linear relations, reminiscent of Ohm's

law, follows a similar structure that includes continuity and diffusion equations. In Sec. III D we combine the relations derived in Secs. III A–III C to obtain expressions for the linear conductivities  $\sigma_{ji}^{xx}(\omega)$  and  $\sigma_{ji}^{yy}(\omega)$  in terms of these impedances. We also obtain expressions for the magnetization amplitude and the local temperature at the F|N interfaces and the spin and heat currents through the interfaces. Finally, in Sec. III E, we numerically evaluate the results for a Pt|YIG|Pt trilayer. Our treatment of charge and spin currents in the normal metals, spin currents through the interfaces, and spin transport through the ferromagnetic insulator by coherent magnons closely follows that of Ref. 52. The treatment of spin and heat transport by thermal magnons is similar to Refs. 18, 34, 51, 62–64.

### A. Normal metal

Transport of charge and spin in the normal metals N1 and N2 is coupled via the spin-Hall effect and the inverse spin-Hall effect. To linear order in the applied field and the induced potential gradients, the charge current densities  $i^{x,y}(z, \omega)$  and the spin current density  $\mathbf{i}_s(z, \omega)$  satisfy the phenomenological response equations [3, 4, 65, 66]

$$i^x(z, \omega) = \sigma_{Ni} E_i(\omega) - \theta_{SHi} \frac{\sigma_{Ni}}{2} \frac{\partial}{\partial z} u_{sy}(z, \omega), \quad (11)$$

$$i^y(z, \omega) = \theta_{SHi} \frac{\sigma_{Ni}}{2} \frac{\partial}{\partial z} u_{sx}(z, \omega), \quad (12)$$

$$\mathbf{i}_s(z, \omega) = -\frac{\sigma_{Ni}}{2} \frac{\partial}{\partial z} \mathbf{u}_s(z, \omega) - \theta_{SHi} \sigma_{Ni} E_i(\omega) \mathbf{e}_y, \quad (13)$$

where we write the indices  $i = 1, 2$  in accordance with the position  $z$  in N1 or N2. Here,  $\theta_{SHi}$  is the spin-Hall angle and  $\sigma_{Ni}$  the electrical conductivity of layer  $Ni$ . The spin accumulation also determines the spin density  $\rho_{es}(z, \omega)$ ,

$$\rho_{es}(z, \omega) = e^2 \nu_{Ni} \mathbf{u}_s(z, \omega), \quad (14)$$

where  $\nu_{Ni}$  is the electronic density of states in  $Ni$ ,  $i = 1, 2$ . (The spin density is measured in equivalent charge units, see the discussion in Sec. II.) Spin current and spin density satisfy the continuity equation

$$-i\omega \rho_{es}(z, \omega) + \frac{\partial}{\partial z} \mathbf{i}_s(z, \omega) = -g_{e\mu, i} \mathbf{u}_s(z, \omega), \quad (15)$$

where

$$g_{e\mu, i} = e^2 \frac{\nu_{Ni}}{\tau_{sf, i}}, \quad (16)$$

with  $\tau_{sf, i}$  the spin flip time in  $Ni$ . Combining Eqs. (13)–(16), one finds that the spin accumulation satisfies

$$\frac{\partial^2}{\partial z^2} \mathbf{u}_s(z, \omega) = \frac{1}{\lambda_{Ni}(\omega)^2} \mathbf{u}_s(z, \omega), \quad (17)$$

where

$$\lambda_{Ni}(\omega)^2 = \frac{\sigma_{Ni}}{2e^2 \nu_{Ni} (1/\tau_{sf, i} - i\omega)} \quad (18)$$

is the spin relaxation length in  $Ni$ ,  $i = 1, 2$ . We will only consider frequencies  $\omega \ll 1/\tau_{sf, i}$  and, hence, neglect the frequency dependence of  $\lambda_{Ni}$  throughout.

We assume that  $\lambda_{Ni}$  is much smaller than the thickness  $d_{Ni}$  of each normal metal layer, so that only the spin accumulations  $\mathbf{u}_{si}(\omega)$  at the interfaces between F and  $Ni$  at  $z = 0$  (for  $i = 1$ ) and  $z = -d_F$  (for  $i = 2$ ) contribute to the inverse spin-Hall effect. From Eqs. (11) and (12) one then finds that the spatially averaged corrections to the charge current densities in N1 and N2 read

$$\delta \bar{i}_i^x(\omega) = (-1)^{i-1} \theta_{SHi} \frac{\sigma_{Ni}}{2d_{Ni}} u_{siy}(\omega), \quad (19)$$

$$\delta \bar{i}_i^y(\omega) = -(-1)^{i-1} \theta_{SHi} \frac{\sigma_{Ni}}{2d_{Ni}} u_{six}(\omega), \quad i = 1, 2, \quad (20)$$

whereas Eq. (13) gives a relationship between the spin voltage  $\mathbf{u}_{si}(\omega)$  and the spin current  $\mathbf{i}_{si}(\omega)$  at the interface,

$$(-1)^{i-1} \mathbf{u}_{si}(\omega) = Z_{Ni} [\mathbf{i}_{si}(\omega) + \theta_{SHi} \sigma_{Ni} E_i(\omega) \mathbf{e}_y], \quad (21)$$

where the “spin impedance”  $Z_{Ni}$ ,  $i = 1, 2$ , is [52]

$$Z_{Ni} = \frac{2\lambda_{Ni}}{\sigma_{Ni}}. \quad (22)$$

At the ferromagnet–normal-metal interfaces, spin and heat transport is coupled (see Sec. III B). To describe heat transport in N1 and N2, we use the continuity equation for the energy density  $(k_B T/2e) \rho_{eQ}(z, t)$  and heat current density  $(k_B T/2e) i_Q^z(z, t)$  of the conduction electrons (both measured in equivalent charge units, see Eq. (4)),

$$-i\omega \rho_{eQ}(z, \omega) + \frac{\partial}{\partial z} i_Q^z(z, \omega) = -g_{eQ, i} \Delta u_{eQ}(z, \omega) + (2e/k_B T) s(z, \omega), \quad (23)$$

where  $\Delta u_{eQ}(z, \omega) = (k_B/e) \Delta T_e$  is the difference of the electronic temperature and the lattice temperature  $T$  (again measured in charge units, see Eq. (5)), which is assumed to be constant throughout, and  $g_{eQ, i}$  is a constant describing the energy exchange with the lattice,

$$g_{eQ, i} = \frac{2e^2}{k_B^2 T} \frac{C_{ei}}{\tau_{ep, i}}. \quad (24)$$

Here,  $C_{ei}$  is the electronic heat capacity and  $\tau_{ep, i}$  the characteristic electron-phonon relaxation time in  $Ni$ ,  $i = 1, 2$ . The Joule heating term  $s(z, \omega)$  on the r.h.s. of Eq. (23) is quadratic in the applied electric field and may be neglected for the linear-response theory. (It will be considered in Sec. IV, where nonlinear response is discussed.) The energy density  $\rho_{eQ}(z, \omega)$  is related to the electron temperature, while the heat current density  $i_Q^z(z, \omega)$  is proportional to its gradient,

$$\rho_{eQ}(z, \omega) = \frac{2e^2}{k_B^2 T} C_{ei} \Delta u_{eQ}(z, \omega), \quad (25)$$

$$i_Q^z(z, \omega) = -\frac{2e^2}{k_B^2 T} \kappa_{ei} \frac{\partial}{\partial z} \Delta u_{eQ}(z, \omega), \quad (26)$$

with  $\kappa_{ei}$  the electronic heat conductivity in Ni,  $i = 1, 2$ . Omitting the Joule heating term, Eq. (23) then becomes

$$\frac{\partial^2}{\partial z^2} \Delta u_{eQ}(z, \omega) = \frac{1}{l_{ep,i}(\omega)^2} \Delta u_{eQ}(z, \omega), \quad (27)$$

with the thermal relaxation length

$$l_{ep,i}(\omega)^2 = \frac{\kappa_{ei}}{C_{ei}(1/\tau_{ep,i} - i\omega)}, \quad i = 1, 2. \quad (28)$$

With the boundary conditions that the heat currents vanish at the interfaces with vacuum at  $z = d_{N1}$  and  $z = -d_{N2} - d_F$ , we find that the excess electron temperature  $\Delta u_{eQ_i}$  and the electronic heat current  $i_{Q_i}$  at the two ferromagnet-normal-metal interfaces  $i = 1, 2$  are related as

$$(-1)^{i-1} \Delta u_{eQ_i}(\omega) = Z_{QN_i}(\omega) i_{Q_i}(\omega), \quad (29)$$

where

$$Z_{QN_i}(\omega) = \frac{k_B^2 T l_{ep,i}(\omega)}{2e^2 \kappa_{ei}} \coth \frac{d_{N_i}}{l_{ep,i}(\omega)} \quad (30)$$

is a “thermal impedance”.

## B. F—N interfaces

In the ferromagnetic insulator F, the spin current  $\mathbf{i}_s(z, t)$  is carried by magnons. It has a coherent transverse component related to the magnetization dynamics as well as an incoherent longitudinal component carried by thermal magnons.

The transverse component  $i_{si\perp}(\omega)$  of the spin current across the ferromagnet-normal-metal interface  $i = 1, 2$  depends on the transverse component  $m_{\perp i}(\omega)$  of the magnetization and the transverse component  $u_{si\perp}(\omega)$  of the spin accumulation in the normal metal. In linear response, the equation for the transverse components of the spin currents across the F|N interfaces are [29, 67]

$$u_{si\perp}(\omega) + \frac{\hbar\omega}{e} m_{\perp i}(\omega) = -(-1)^{i-1} Z_{FNi\perp} i_{si\perp}(\omega). \quad (31)$$

Here,  $Z_{FNi\perp}$  is the interfacial spin impedance [52]

$$Z_{FNi\perp} = \frac{1}{g_{\uparrow\downarrow i}}, \quad (32)$$

where  $g_{\uparrow\downarrow i}$  is the spin-mixing conductance per unit area of the F|Ni interface,  $i = 1, 2$ .

The interfacial longitudinal spin current depends not only on the magnon chemical potential  $u_{mi}$  and the longitudinal component  $u_{si\parallel}$  of the spin accumulation at the interface, but, via the interfacial spin-Seebeck effect, also on the difference  $u_{eQ_i} - u_{mQ_i}$  of electron and magnon temperatures across the interface. At the same time, a temperature and/or chemical potential difference also

causes a heat current through the interface. The longitudinal spin current and the heat current at the two interfaces are given by the relation [34, 52]

$$\begin{pmatrix} u_{si\parallel} - u_{mi} \\ \Delta u_{eQ_i} - \Delta u_{mQ_i} \end{pmatrix} = -(-1)^{i-1} \mathcal{Z}_{FNi\parallel} \begin{pmatrix} i_{si\parallel} \\ i_{Q_i} \end{pmatrix}, \quad (33)$$

where  $\mathcal{Z}_{FNi\parallel}$  is the interfacial impedance matrix,

$$\mathcal{Z}_{FNi\parallel}^{-1} = \frac{3k_T^3 \text{Re} g_{\uparrow\downarrow i}}{16\pi^{3/2} s} \begin{pmatrix} 4\zeta(3/2) & 10\zeta(5/2) \\ 10\zeta(5/2) & 35\zeta(7/2) \end{pmatrix}. \quad (34)$$

Here,  $k_T$  is the thermal magnon wave number,

$$k_T = \sqrt{\frac{k_B T}{\hbar D_{\text{ex}}}} \quad (35)$$

with the equilibrium temperature  $T$ ,  $s$  is the equilibrium spin density in F, and  $\zeta$  the Riemann zeta function. Note that all four elements of the  $2 \times 2$  impedance matrix  $\mathcal{Z}_{FNi\parallel}$  have the same units, because spin and heat currents, as well as spin accumulation and temperature, are measured in the same units.

## C. Ferromagnetic insulator

It remains to find expressions linking the magnon chemical potentials  $u_{m1}(\omega)$  and  $u_{m2}(\omega)$  and the magnetization amplitudes  $m_{\perp 1}$  and  $m_{\perp 2}$  to the spin currents at the two F|N interfaces. For the thermal magnons, we employ a phenomenological description of magnon-mediated spin and heat transport, while the coherent magnons are described by the microscopic Landau-Lifshitz-Gilbert equation.

### 1. Coherent magnons

The transverse magnetization amplitude  $m_{\perp}(z, \omega)$  satisfies the linearized Landau-Lifshitz-Gilbert equation,

$$-D_{\text{ex}} \frac{\partial^2}{\partial z^2} m_{\perp}(z, \omega) = (\omega + i\alpha\omega - \omega_0) m_{\perp}(z, \omega), \quad (36)$$

where  $\omega_0$  is the ferromagnetic-resonance frequency, which includes effects of static external magnetic fields, the demagnetization field, and anisotropies;  $D_{\text{ex}}$  is the spin stiffness, and  $\alpha$  the bulk Gilbert damping coefficient. The transverse spin current is given by

$$j_{s\perp}^z(z, \omega) = i\hbar D_{\text{ex}} s \frac{\partial}{\partial z} m_{\perp}(z, \omega). \quad (37)$$

Solving Eq. (36) with the boundary conditions  $m_{\perp}(0, \omega) = m_{\perp 1}(\omega)$ ,  $m_{\perp}(-d_F, \omega) = m_{\perp 2}(\omega)$ , we find

$$m_{\perp}(z, \omega) = \frac{m_{\perp 1}(\omega) \sin(k(\omega)(z + d_F))}{\sin(k(\omega)d_F)} - \frac{m_{\perp 2}(\omega) \sin(k(\omega)z)}{\sin(k(\omega)d_F)}, \quad (38)$$



where  $k(\omega)$  is the magnon wavenumber at frequency  $\omega$ ,

$$k(\omega)^2 = \frac{\omega(1 + i\alpha) - \omega_0}{D_{\text{ex}}}. \quad (39)$$

For definiteness, in expressions that contain  $k(\omega)$ , we choose the sign of  $k(\omega)$  such that  $\text{Im } k(\omega) > 0$ . Combining Eqs. (37) and (38), one obtains a relation between the transverse spin currents and the transverse magnetization amplitudes at the two ferromagnet–normal-metal interfaces,

$$\begin{aligned} (-1)^{i-1} (\hbar\omega/e) [m_{\perp i}(\omega) \cos(k(\omega)d_F) - m_{\perp j}(\omega)] \\ = -iZ_{F\perp}^\infty(\omega) i_{si\perp}(\omega) \sin(k(\omega)d_F), \quad i \neq j, \end{aligned} \quad (40)$$

where

$$Z_{F\perp}^\infty(\omega) = \frac{\hbar\omega}{2e^2 D_{\text{ex}} k(\omega) s}. \quad (41)$$

## 2. Thermal magnons

Following Cornelissen *et al.* [34] we describe thermal magnons in F in terms of the magnon chemical potential  $\mu_m(z, t) = eu_m(z, t)$  and the difference  $\Delta T_m(z, t) = T_m(z, t) - T = (e/k_B)\Delta u_{mQ}(z, t)$  of the magnon temperature and the lattice temperature. To linear order in  $u_m(z, t)$  and  $\Delta u_{mQ}(z, t)$ , the deviations of the magnon spin density  $(\hbar/2e)\rho_{ms}(z, t)$  and the magnon energy density  $(k_B T/2e)\rho_{mQ}(z, t)$  from their equilibrium values (both measured in charge units) can be expanded in the form

$$\begin{pmatrix} \Delta\rho_{ms}(z, t) \\ \Delta\rho_{mQ}(z, t) \end{pmatrix} = \mathcal{C}_m \begin{pmatrix} u_m(z, t) \\ \Delta u_{mQ}(z, t) \end{pmatrix}, \quad (42)$$

where

$$\mathcal{C}_m = \begin{pmatrix} c_{m,s\mu} & c_{m,sT} \\ c_{m,Q\mu} & c_{m,QT} \end{pmatrix} \quad (43)$$

is a  $2 \times 2$  matrix with  $c_{m,Q\mu} = c_{m,sT}$  and  $c = (k_B^2 T/2e^2) c_{m,QT}/\rho_{\text{YIG}}$  constitutes the specific magnon heat capacity. Expressions for the four elements of the matrix  $\mathcal{C}_m$  in terms of the magnon density of states and the magnon distribution function are given in App. A. The magnon spin density and magnon energy density satisfy the continuity equation

$$\begin{aligned} \frac{\partial}{\partial t} \begin{pmatrix} \Delta\rho_{ms}(z, t) \\ \Delta\rho_{mQ}(z, t) \end{pmatrix} + \frac{\partial}{\partial z} \begin{pmatrix} i_{s\parallel}(z, t) \\ i_Q(z, t) \end{pmatrix} \\ = -\mathcal{G}_m \begin{pmatrix} u_m(z, t) \\ \Delta u_{mQ}(z, t) \end{pmatrix}, \end{aligned} \quad (44)$$

where,  $i_{s\parallel}(z, t)$  and  $i_Q(z, t)$  are the magnon spin current and the magnon heat current and

$$\mathcal{G}_m = \begin{pmatrix} g_{m,s\mu} & g_{m,sT} \\ g_{m,Q\mu} & g_{m,QT} \end{pmatrix} \quad (45)$$

is a  $2 \times 2$  matrix describing various forms of spin and energy relaxation of magnons, which will be described in more detail below. The magnon spin and heat current densities depend linearly on gradients of the magnon chemical potential and the magnon temperature,

$$\begin{pmatrix} i_{s\parallel}(z, \omega) \\ i_Q(z, \omega) \end{pmatrix} = -\Sigma_m(\omega) \frac{\partial}{\partial z} \begin{pmatrix} u_m(z, \omega) \\ \Delta u_{mQ}(z, \omega) \end{pmatrix}, \quad (46)$$

where [34]

$$\Sigma_m(\omega) = \frac{1}{1 - i\omega\tau_m} \begin{pmatrix} \sigma_m & eL_m/k_B T \\ eL_m/k_B T & 2e^2 \kappa_m/k_B^2 T \end{pmatrix}, \quad (47)$$

with the magnon spin conductivity  $\sigma_m$ , the bulk spin-Seebeck coefficient  $L_m$ , and the magnon heat conductivity  $\kappa_m$ . The time  $\tau_m$  is a relaxation time for momentum relaxation of magnons, which will be described in more detail below. Expressions relating  $\sigma_m$ ,  $L_m$ , and  $\kappa_m$  to the relaxation time  $\tau_m$  are given in App. A. Numerical estimates for YIG, based on material parameters listed in Tab. I, can be found in Tab. II.

The Fourier transform of Eq. (44), in combination with Eqs. (42) and (46), yields coupled diffusion equations for magnon heat transport and longitudinal magnon spin transport. These equations may be written in the form

$$\frac{\partial^2}{\partial z^2} \begin{pmatrix} u_m \\ \Delta u_{mQ} \end{pmatrix} = \Lambda(\omega)^{-2} \begin{pmatrix} u_m \\ \Delta u_{mQ} \end{pmatrix}, \quad (48)$$

with

$$\Lambda^2(\omega) = (\mathcal{G}_m - i\omega\mathcal{C}_m)^{-1} \Sigma(\omega). \quad (49)$$

The matrix  $\Lambda(\omega)$  describes the relaxation lengths for magnon spin and energy density. It is a  $2 \times 2$  matrix, because spin and energy transport by magnons is coupled. We choose the sign of  $\Lambda(\omega)$  such that  $\text{Re } l_m(\omega) > 0$  for the two eigenvalues  $l_m(\omega)$  of  $\Lambda(\omega)$ ,  $m = 1, 2$ .

The relaxation times for magnons can be attributed to exchange-based spin-conserving magnon–magnon interactions, spin-conserving magnon–phonon scattering, relativistic spin-non-conserving magnon–magnon interactions, spin-non-conserving magnon–phonon scattering (including relaxation processes involving magnon–polaron formation), and elastic magnon–impurity scattering. We denote the relaxation times for these processes  $\tau_{m,\text{ex}}$ ,  $\tau_{\text{mp},\text{ex}}$ ,  $\tau_{m,\text{rel}}$ ,  $\tau_{\text{mp},\text{rel}}$ , and  $\tau_{m,\text{el}}$ , respectively.

In the framework of the relaxation time approximation, the relaxation constants in the phenomenological magnon transport equations shown above can be expressed in terms of the relaxation times for these fundamental scattering processes,

$$\begin{aligned} \mathcal{G}_m = \mathcal{C}_m \tau_{\text{mp},\text{rel}}^{-1} \\ + (1 - \gamma) \begin{pmatrix} c_{m,s\mu} \tau_{m,\text{rel}}^{-1} & 0 \\ 0 & c_{m,QT} \tau_{\text{mp},\text{ex}}^{-1} \end{pmatrix}, \end{aligned} \quad (50)$$

with

$$\gamma = \frac{c_{m,sT} c_{m,Q\mu}}{c_{m,s\mu} c_{m,QT}}, \quad (51)$$

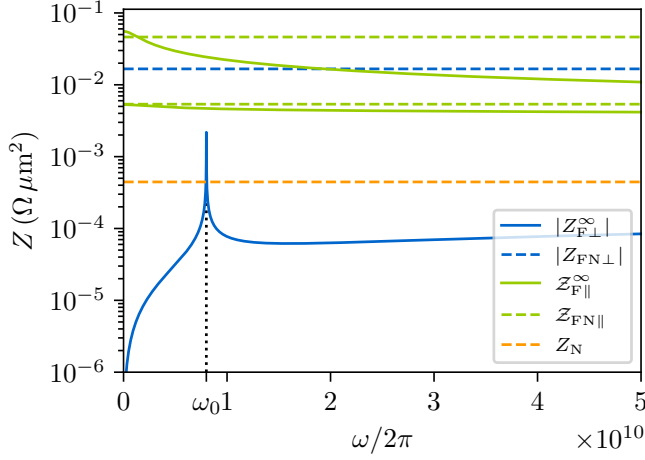


FIG. 2. Spin impedances defined in Eqs. (22), (32), (34), (41), and (55) for a Pt|YIG|Pt trilayer. For the matrix impedances  $Z_{FN\parallel}$  and  $Z_{F\parallel}^{\infty}$ , this figure shows the absolute values of the two eigenvalues. The interface impedances dominate the spin transport except at low frequency, where a magnon chemical potential builds up in F, which results in a large longitudinal magnon impedance. Material and device parameters are taken from Tabs. I and II.

and the total momentum relaxation time  $\tau_m$  in Eq. (47) becomes

$$\tau_m^{-1} = \tau_{m,\text{ex}}^{-1} + \tau_{m,\text{rel}}^{-1} + \tau_{\text{mp},\text{ex}}^{-1} + \tau_{\text{mp},\text{rel}}^{-1} + \tau_{m,\text{el}}^{-1}. \quad (52)$$

We refer to App. A for details.

The solution of Eq. (48) can then be written in a form similar to Eq. (38),

$$\begin{pmatrix} u_m(z) \\ \Delta u_{mQ}(z) \end{pmatrix} = \frac{\sinh(\Lambda(\omega)^{-1}(z + d_F))}{\sinh(\Lambda(\omega)^{-1}d_F)} \begin{pmatrix} u_{m1} \\ \Delta u_{mQ1} \end{pmatrix} - \frac{\sinh(\Lambda(\omega)^{-1}z)}{\sinh(\Lambda(\omega)^{-1}d_F)} \begin{pmatrix} u_{m2} \\ \Delta u_{mQ2} \end{pmatrix}, \quad (53)$$

where we recall that  $u_{m1} = u_m(0)$ ,  $u_{m2} = u_m(-d_F)$ ,  $\Delta u_{mQ1} = \Delta u_{mQ}(0)$ , and  $\Delta u_{mQ2} = \Delta u_{mQ}(-d_F)$  refer to values taken at the interfaces with the normal metals N1 and N2. From Eq. (46) and Eq. (53), we relate spin and heat currents with the magnon chemical potential and the magnon temperature,

$$\begin{aligned} & (-1)^{i-1} \cosh(\Lambda(\omega)^{-1}d_F) \begin{pmatrix} u_{mi} \\ \Delta u_{mQi} \end{pmatrix} - \begin{pmatrix} u_{mj} \\ \Delta u_{mQj} \end{pmatrix} \\ & = -\sinh(\Lambda(\omega)^{-1}d_F) Z_{F\parallel}^{\infty}(\omega) \begin{pmatrix} i_{si\parallel} \\ i_{Qi} \end{pmatrix} \end{aligned} \quad (54)$$

for  $i \neq j$ , where

$$Z_{F\parallel}^{\infty}(\omega) = \Lambda(\omega)\Sigma(\omega)^{-1}. \quad (55)$$

#### D. Conductivity corrections

In the previous sections, we established linear relations between current and voltage equivalents. These relations constitute a system of equations, from which we can deduce the linear response of a charge current to an applied electric field. Solving the coupled Equations (21), (31), and (40) for the transverse components of the spin current densities  $\mathbf{i}_{sj}$  through each interface  $j = 1, 2$ , we find

$$i_{sj\perp}(\omega) = -\sum_{i=1}^2 \theta_{\text{SH}i} \sigma_{Ni} \frac{Z_{Ni}}{Z_{ji\perp}(\omega)} E_i(\omega) \mathbf{e}_{\perp}^* \cdot \mathbf{e}_y, \quad (56)$$

with the total local and nonlocal spin impedances

$$\begin{aligned} Z_{11\perp}(\omega) &= Z_{N1} + Z_{FN1\perp} + [\cos(k(\omega)d_F)(Z_{N2} + Z_{FN2\perp}) - i \sin(k(\omega)d_F)Z_{F\perp}^{\infty}] \\ &\quad \times [\cos(k(\omega)d_F)Z_{F\perp}^{\infty} - i \sin(k(\omega)d_F)(Z_{N2} + Z_{FN2\perp})]^{-1} Z_{F\perp}^{\infty}, \end{aligned} \quad (57)$$

$$\begin{aligned} Z_{21\perp}(\omega) &= (Z_{N1} + Z_{FN1\perp})(Z_{F\perp}^{\infty})^{-1} [\cos(k(\omega)d_F)Z_{F\perp}^{\infty} - i \sin(k(\omega)d_F)(Z_{N2} + Z_{FN2\perp})] \\ &\quad + \cos(k(\omega)d_F)(Z_{N2} + Z_{FN2\perp}) - i \sin(k(\omega)d_F)Z_{F\perp}^{\infty}, \end{aligned} \quad (58)$$

where we omitted the frequency dependence of  $Z_{F\perp}^{\infty}(\omega)$  for brevity. The effective impedance  $Z_{12\perp}(\omega) = Z_{21\perp}(\omega)$  and  $Z_{22\perp}(\omega)$  is obtained from Eq. (57) by interchanging the indices  $1 \leftrightarrow 2$ . Note that  $Z_{ii\perp}(\omega \rightarrow 0) = Z_{Ni} + Z_{FNi\perp}$  since  $Z_{F\perp}^{\infty}(0) = 0$ .

To find the longitudinal component of the spin current and the heat current at the interfaces we proceed in a similar manner. Since the impedances  $Z_{Fj\parallel}(\omega)$  and  $Z_{FNj\parallel}(\omega)$  are  $2 \times 2$  matrices describing combined spin and heat transport, we also define

$$Z_{Nj}(\omega) = \begin{pmatrix} Z_{Nj} & 0 \\ 0 & Z_{QNj}(\omega) \end{pmatrix}. \quad (59)$$

From Eqs. (29), (21), (33), and (54) we then obtain

$$\begin{pmatrix} i_{sj\parallel}(\omega) \\ i_{Qj}(\omega) \end{pmatrix} = - \sum_{i=1}^2 \theta_{\text{SH}i} \sigma_{\text{Ni}} Z_{\text{Ni}} \mathcal{Z}_{ji}^{-1}(\omega) \begin{pmatrix} E_i(\omega) \\ 0 \end{pmatrix} \mathbf{m}_{\text{eq}} \cdot \mathbf{e}_y, \quad (60)$$

with the effective impedances

$$\begin{aligned} \mathcal{Z}_{11\parallel}(\omega) &= \mathcal{Z}_{\text{N}1} + \mathcal{Z}_{\text{FN}1\parallel} + \left[ \sinh(\Lambda(\omega)^{-1} d_{\text{F}}) \mathcal{Z}_{\text{F}\parallel}^{\infty} + \cosh(\Lambda(\omega)^{-1} d_{\text{F}}) (\mathcal{Z}_{\text{N}2} + \mathcal{Z}_{\text{FN}2\parallel}) \right] \\ &\quad \times \left[ \cosh(\Lambda(\omega)^{-1} d_{\text{F}}) \mathcal{Z}_{\text{F}\parallel}^{\infty} + \sinh(\Lambda(\omega)^{-1} d_{\text{F}}) (\mathcal{Z}_{\text{N}2} + \mathcal{Z}_{\text{FN}2\parallel}) \right]^{-1} \mathcal{Z}_{\text{F}\parallel}^{\infty}, \end{aligned} \quad (61)$$

$$\begin{aligned} \mathcal{Z}_{21\parallel}(\omega) &= (\mathcal{Z}_{\text{N}1} + \mathcal{Z}_{\text{FN}1\parallel}) (\mathcal{Z}_{\text{F}\parallel}^{\infty})^{-1} \left[ \cosh(\Lambda(\omega)^{-1} d_{\text{F}}) \mathcal{Z}_{\text{F}\parallel}^{\infty} + \sinh(\Lambda(\omega)^{-1} d_{\text{F}}) (\mathcal{Z}_{\text{N}2} + \mathcal{Z}_{\text{FN}2\parallel}) \right] \\ &\quad + \sinh(\Lambda(\omega)^{-1} d_{\text{F}}) \mathcal{Z}_{\text{F}\parallel}^{\infty} + \cosh(\Lambda(\omega)^{-1} d_{\text{F}}) (\mathcal{Z}_{\text{N}2} + \mathcal{Z}_{\text{FN}2\parallel}). \end{aligned} \quad (62)$$

Here we omitted the frequency arguments of the spin impedances for clarity. The effective impedances  $\mathcal{Z}_{12\parallel}(\omega)$  and  $\mathcal{Z}_{22\parallel}(\omega)$  are obtained from Eqs. (61) and (62) by interchanging the indices  $1 \leftrightarrow 2$ . Using Eq. (21) we may then calculate the longitudinal and transverse components of the spin accumulations,  $\mathbf{u}_{s1}(\omega)$  and  $\mathbf{u}_{s2}(\omega)$ ,

$$\begin{aligned} \mathbf{u}_{sj}(\omega) &= \frac{2\lambda_{\text{N}j}}{\sigma_{\text{N}j}} \sum_{i=1}^2 \theta_{\text{SH}i} \sigma_{\text{N}i} E_i(\omega) (-1)^{i-1} \\ &\quad \times \left[ \delta_{ji} \mathbf{e}_y - \zeta_{ji\parallel}(\omega) (\mathbf{e}_y \cdot \mathbf{m}_{\text{eq}}) \mathbf{m}_{\text{eq}} - \zeta_{ji\perp}(\omega) (\mathbf{e}_y \cdot \mathbf{e}_{\perp}^*) \mathbf{e}_{\perp} - \zeta_{ji\perp}(-\omega)^* (\mathbf{e}_y \cdot \mathbf{e}_{\perp}) \mathbf{e}_{\perp}^* \right], \end{aligned} \quad (63)$$

where the coefficients  $\zeta_{ji\perp}(\omega)$  and  $\zeta_{ji\parallel}(\omega)$  are defined as

$$\zeta_{ji\perp}(\omega) = \frac{Z_{\text{N}i}}{Z_{ji\perp}(\omega)}, \quad (64)$$

$$\zeta_{ji\parallel}(\omega) = Z_{\text{N}i} \left[ \mathcal{Z}_{ji\parallel}^{-1}(\omega) \right]_{s\mu}. \quad (65)$$

In this expression, the subscript “ $s\mu$ ” points to the upper left element in the  $2 \times 2$  impedance matrix, similar to the notation introduced in Eq. (43). The local and nonlocal SMR effect then results in the conductivities

$$\frac{\sigma_{ji}^{xx}(\omega)}{\sigma_{\text{N}i}} = \delta_{ji} + \frac{\lambda_{\text{N}j}}{2d_{\text{N}j}} [s_{ji}(\omega)(1 - m_y^2) + s'_{ji}(\omega)], \quad (66)$$

$$\frac{\sigma_{ji}^{yx}(\omega)}{\sigma_{\text{N}i}} = \frac{\lambda_{\text{N}j}}{2d_{\text{N}j}} [s_{ji}(\omega)m_x m_y + s''_{ji}(\omega)m_z], \quad (67)$$

where we used Eqs. (6) and (8) for the unit vectors  $\mathbf{m}_{\text{eq}}$  and  $\mathbf{e}_{\perp}$  and

$$\begin{aligned} s_{ji}(\omega) &= \theta_{\text{SH}j} \theta_{\text{SH}i} [2\zeta_{ji\parallel}(\omega) - \zeta_{ji\perp}(\omega) - \zeta_{ji\perp}(-\omega)^*], \\ s'_{ji}(\omega) &= -2\theta_{\text{SH}j} \theta_{\text{SH}i} \zeta_{ji\parallel}(\omega), \\ s''_{ji}(\omega) &= -i\theta_{\text{SH}j} \theta_{\text{SH}i} [\zeta_{ji\perp}(\omega) - \zeta_{ji\perp}(-\omega)^*] \end{aligned} \quad (68)$$

are dimensionless coefficients describing contributions to the conductivity with different characteristic dependences on the magnetization direction  $\mathbf{m}_{\text{eq}}$ . These equations are the central results of this Section. They generalize the theory of Ref. 52 to the nonlocal response. The term proportional to  $m_x m_y$ , with the dimensionless off-diagonal conductivity coefficient  $s_{11}^{xy}$ , can be identified with a spin-Hall version of the planar Hall effect, which

is symmetric under magnetization reversal. The terms proportional to  $m_z$  correspond to a spin-Hall version of the anomalous Hall effect, which is antisymmetric under magnetization reversal.

For future reference, we also give expressions for the electronic excess temperature  $\Delta u_{\text{eQ}j}$ , the heat current  $i_{\text{Q}j}^z$ , and the magnetization amplitude  $m_{\perp j}$  at the interface between F and Nj,

$$\Delta u_{\text{eQ}j}(\omega) = -(-1)^{j-1} \quad (69)$$

$$\times \sum_{i=1}^2 Z_{\text{N}i} \theta_{\text{SH}i} \sigma_{\text{N}i} \Phi_{ji}(\omega) E_i(\omega) \mathbf{m}_{\text{eq}} \cdot \mathbf{e}_y,$$

$$i_{\text{Q}j}(\omega) = - \sum_{i=1}^2 \theta_{\text{SH}i} \sigma_{\text{N}i} \phi_{ji}(\omega) E_i(\omega) \mathbf{m}_{\text{eq}} \cdot \mathbf{e}_y, \quad (70)$$

$$\begin{aligned} m_{\perp j}(\omega) &= -(-1)^{i-1} \\ &\quad \times \sum_{i=1}^2 \eta_{ji\perp}(\omega) \frac{\theta_{\text{SH}i} \sigma_{\text{N}i}}{2i_{\text{F}}} E_i(\omega) \mathbf{e}_{\perp}^* \cdot \mathbf{e}_y, \end{aligned} \quad (71)$$

where

$$i_{\text{F}} = es\sqrt{D_{\text{ex}}\omega_0} \quad (72)$$



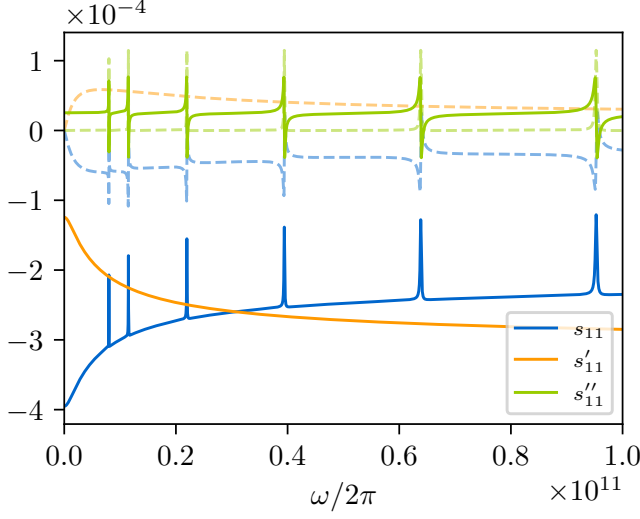


FIG. 3. Real part (solid line) and imaginary part (dashed line) of local linear response coefficients  $s_{11}(\omega)$  (blue),  $s'_{11}(\omega)$  (orange), and  $s''_{11}(\omega)$  (green), see Eq. (68). The three dimensionless coefficients have a different dependence on the direction of the magnetization in F and characterize the local conductivity correction from the coupling of N to F|N. We note that the coefficient  $s_{11}(\omega)$  is directly proportional to the SMR response calculated in Ref. 52, while  $s''_{11}(\omega)$  describes the anomalous Hall effect (AHE).

has the dimension of “charge current density” and

$$\Phi_{ji}(\omega) = Z_{QNj}(\omega) \left[ Z_{ji\parallel}^{-1}(\omega) \right]_{Q\mu}, \quad (73)$$

$$\phi_{ji}(\omega) = Z_{Ni} \left[ Z_{ji\parallel}^{-1}(\omega) \right]_{Q\mu}, \quad (74)$$

$$\eta_{ji\perp}(\omega) = \frac{Z_{Ni}}{Z_{F\perp}^{\infty}(\omega)} \left( \delta_{ij} - (-1)^{i+j} \frac{Z_{Nj} + Z_{FNj\perp}}{Z_{ji\perp}(\omega)} \right) \times \sqrt{\frac{\omega_0}{\omega(1+i\alpha) - \omega_0}}, \quad (75)$$

are dimensionless coefficients, where the indices “Q” and “ $\mu$ ” in Eqs. (73) and (74) refer to the  $2 \times 2$  matrix structure defined in Eqs. (33) and (34) with the notation introduced in Eq. (43).

### E. Numerical estimates and discussion

We now present characteristic results for the local and nonlocal spin-Hall magnetoresistance effect, using parameters for a Pt|YIG|Pt-trilayer. (We regard the ferromagnet yttrium iron garnet (YIG) as ferromagnetic.) The material and device parameters used are summarized in Tabs. I and II. In Fig. 2 we show (the absolute value of) the transverse impedances  $Z_{F\perp}$  and  $Z_{F\parallel}^{\infty}$  as a function of frequency, as well as (the absolute values of) the eigenvalues of the longitudinal impedances  $Z_N$ ,  $Z_{F\parallel}$  and  $Z_{F\parallel}^{\infty}$ , using the parameters from Tabs. I and

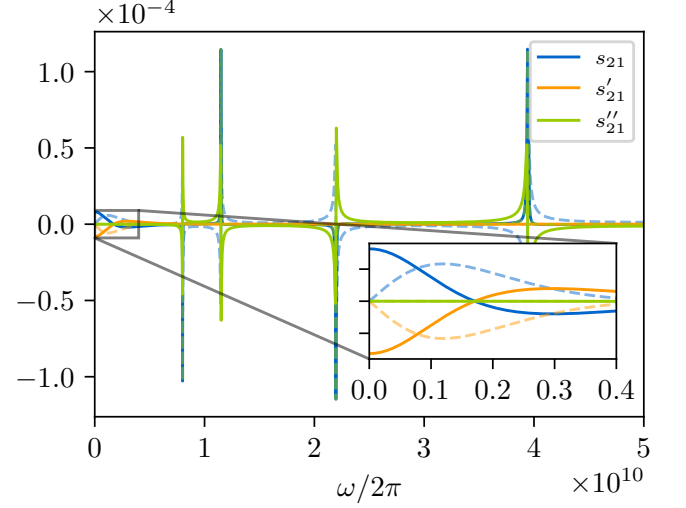


FIG. 4. Real part (solid line) and imaginary part (dashed line) of nonlocal linear response coefficients  $s_{21}(\omega)$  (blue),  $s'_{21}(\omega)$  (orange), and  $s''_{21}(\omega)$  (green), see Eq. (68). At low frequency, the nonlocal conductivity is mediated by thermal magnons, but coherent spin waves dominate at GHz to THz frequencies.

II. We assume equal properties for the two normal metal layers and for the two interfaces. The dimensionless coefficients  $s_{ji}(\omega)$ ,  $s'_{ji}(\omega)$ , and  $s''_{ji}(\omega)$ , which each describe a contribution to the local and nonlocal conductivities with a different characteristic magnetization dependence, are shown in Figs. 3 and 4.

The dimensionless conductivity corrections  $s_{ji}(\omega)$  and  $s''_{ji}(\omega)$  are determined by the transverse and longitudinal effective impedances  $Z_{ji\perp}(\omega)$  and  $Z_{ji\parallel}(\omega)$ , see Eq. (68), whereas the conductivity correction  $s'_{ji}(\omega)$  has a longitudinal contribution only. To gain a qualitative understanding of their frequency dependence, we now discuss the transverse and longitudinal effective impedances  $Z_{ji\perp}(\omega)$  and  $Z_{ji\parallel}(\omega)$  separately.

For the transverse response, the effective impedance  $Z_{ji\perp}(\omega)$  is dominated by the impedances of the two ferromagnet–normal-metal interfaces, except in the vicinity of resonance frequencies

$$\omega_n = D_{\text{ex}} \left( \frac{n\pi}{d_F} \right)^2 + \omega_0 \quad (76)$$

where one may approximate

$$\begin{aligned} Z_{11\perp}(\omega) &\approx Z_{FN1\perp} \\ &+ \frac{Z_{FN2\perp}}{1 - i(-1)^n(\omega - \omega_n) \frac{2e^2 d_F s}{\hbar \omega_n (1 + \delta_{n,0})} Z_{FN2\perp}}, \\ Z_{21\perp}(\omega) &\approx Z_{FN1\perp} + Z_{FN2\perp} \\ &- i(-1)^n(\omega - \omega_n) \frac{2e^2 d_F s Z_{FN1\perp} Z_{FN2\perp}}{\hbar \omega_n (1 + \delta_{n,0})}. \end{aligned} \quad (77)$$

(These expressions neglect the decay of coherent magnons, which is described by the Gilbert damping con-

Quantity	Value	Ref.
$T$	300 K	-
$g_{\uparrow\downarrow}$	$(6 + 0.3i) \times 10^{13} \Omega^{-1} \text{m}^{-2}$	10, 12, and 68
YIG		
$d_F$	$6 \times 10^{-8} \text{m}$	-
$\alpha$	$2 \times 10^{-4}$	21
$\omega_0/2\pi$	$8 \times 10^9 \text{s}^{-1}$	10
$D_{\text{ex}}$	$8 \times 10^{-6} \text{m}^2 \text{s}^{-1}$	69
$a$	$1.2376 \times 10^{-9} \text{m}$	70
$sa^3$	10	70
$\tau_{\text{m,el}}$	0.11 ps	-
$\tau_{\text{m,ex}}$	2.7 ps	71
$\tau_{\text{mp,ex}}$	0.5 ps	34
$\tau_{\text{m,rel}}, \tau_{\text{mp,rel}}$	$2\hbar/(\alpha k_B T) \approx 255 \text{ps}$	-
Pt		
$d_N$	$4 \times 10^{-9} \text{m}$	-
$\theta_{\text{SH}}$	0.1	12
$\lambda_N$	$2 \times 10^{-9} \text{m}$	69
$\sigma_N$	$9 \times 10^6 \Omega^{-1} \text{m}^{-1}$	72
$C_e$	$133 \text{J kg}^{-1} \text{K}^{-1}$	73
$\rho$	$2.15 \times 10^4 \text{kg m}^{-3}$	73
$l_{\text{ep}}$	$4.5 \times 10^{-9} \text{m}$	62 and 69

TABLE I. Material parameters for YIG and Pt.  $\tau_{\text{ep}} \approx 0.9 \text{ps}$  in Eq. (23) is calculated from  $l_{\text{ep}}$  and  $\kappa_e$ , which is in turn calculated from  $\sigma_N$  via the Wiedemann-Franz law. The time scale  $\tau_{\text{m,ex}}$  is mainly associated with “four-magnon scattering” and we estimate the combined  $\tau_{\text{m,rel}}$  and  $\tau_{\text{mp,rel}}$  from the Landau-Lifshitz-Gilbert equation since both processes are not magnon-number conserving. At room temperature, spin-non-conserving “three-magnon scattering” can be neglected in comparison to the spin-conserving “four-magnon scattering” [71]. The impurity scattering  $\tau_{\text{m,el}}$  is fitted to reproduce the magnon conductivity  $\sigma_{\text{m}} \approx 4 \times 10^5 \text{S m}^{-1}$  measured in Ref. 21. A comparison to a microscopical model as discussed in Ref. 35 yields a similar order of magnitude for the relaxation time at room temperature.

stant  $\alpha$  in Eq. (39).) As a result, the transverse contributions to the local and nonlocal response coefficients  $s_{ji}(\omega)$  and  $s''_{ji}(\omega)$  have sharp resonant features in the vicinity of the resonance frequencies, where the sign of the resonant feature alternates between resonances. At frequency  $\omega = 0$ , the transverse contribution to the non-local conductivities is strictly zero.

For the longitudinal response at room temperature,  $\mathcal{Z}_{N1}$  and  $\mathcal{Z}_{N2}$  may also be neglected in comparison to the interfacial impedances  $\mathcal{Z}_{\text{FN1}\parallel}$  and  $\mathcal{Z}_{\text{FN2}\parallel}$ . Furthermore, since the magnon momentum-relaxation time  $\tau_{\text{m}}$  is less than 0.1 ps, the frequency dependence of the conductivity matrix  $\Sigma(\omega)$  may be neglected for  $\omega$  in the THz range and below, so that the frequency dependence of the longitudinal effective impedance  $\mathcal{Z}_{ij\parallel}(\omega)$  is dominated by the two lengths  $l_m(\omega)$ ,  $m = 1, 2$ , for magnon spin and en-

Quantity	Value	Eq.
$l_{\mu}$	20 nm	(80)
$l_T$	7 nm	(81)
$i_F$	$0.54 \text{A } \mu\text{m}^{-2}$	(72)
$i_N$	$340 \text{A } \mu\text{m}^{-2}$	(92)
$i_{\text{FN}}$	$0.43 \text{A } \mu\text{m}^{-2}$	(102)
$\mathcal{G}_{\text{m}}$	$g_{\text{m,s}\mu}$	$11 \times 10^2 \Omega^{-1} \mu\text{m}^{-3}$ (50)
	$g_{\text{m,s}T}$	$45 \times 10^0 \Omega^{-1} \mu\text{m}^{-3}$ (50)
	$g_{\text{m,Q}\mu}$	$45 \times 10^0 \Omega^{-1} \mu\text{m}^{-3}$ (50)
	$g_{\text{m,Q}T}$	$29 \times 10^3 \Omega^{-1} \mu\text{m}^{-3}$ (50)
$\mathcal{C}_{\text{m}}$	$c_{\text{m,s}\mu}$	$150 \text{ns } \Omega^{-1} \mu\text{m}^{-3}$ (A5)
	$c_{\text{m,s}T}$	$11 \text{ns } \Omega^{-1} \mu\text{m}^{-3}$ (A5)
	$c_{\text{m,Q}\mu}$	$11 \text{ns } \Omega^{-1} \mu\text{m}^{-3}$ (A9)
	$c_{\text{m,Q}T}$	$15 \text{ns } \Omega^{-1} \mu\text{m}^{-3}$ (A9)
$c = (k_B^2 T / 2e^2) c_{\text{m,Q}T} / \rho_{\text{YIG}}$	$3.3 \text{J kg}^{-1} \text{K}^{-1}$	(A9)
$\Sigma_{\text{m}}(0)$	$\sigma_{\text{m}}$	$0.41 \Omega^{-1} \mu\text{m}^{-1}$ (A29)
	$eL_{\text{m}}/k_B T$	$0.55 \Omega^{-1} \mu\text{m}^{-1}$ (A30)
	$eL_{\text{m}}/k_B T$	$0.55 \Omega^{-1} \mu\text{m}^{-1}$ (A30)
	$2e^2 \kappa_{\text{m}} / k_B^2 T$	$1.63 \Omega^{-1} \mu\text{m}^{-1}$ (A31)
$\sigma_{\text{m}}$	$4.1 \times 10^5 \text{S m}^{-1}$	(A29)
$L$	$1.4 \times 10^4 \text{A m}^{-1}$	(A30)
$\kappa_{\text{m}}$	$1.8 \text{W K}^{-1} \text{m}^{-1}$	(A31)

TABLE II. Derived quantities for YIG from the Boltzmann theory in App. A and the characteristic charge current densities  $i_F$ ,  $i_{\text{FN}}$ , and  $i_N$ , which set the scale for the three bilinear processes discussed in Sec. IV. The characteristic length scales associated with magnon transport mediated (mainly) by the magnon chemical potential or magnon temperature are the eigenvalues of  $\Lambda$ , Eq. (49), at zero frequency,  $l_1 \sim l_{\mu}$  and  $l_2 \sim l_T$ , respectively (see Sec. III E). As Ref. 34, our model suggests that the magnon chemical potential carries farther than the magnon temperature. In general, Refs. 21, 34, and 51 suggest a longer magnon spin diffusion length than the value listed here. We attribute this difference to a shortcoming of the relaxation time approximation in the Boltzmann theory that neglects subthermal magnon transport, as discussed in Ref. 74.

ergy relaxation, which are the two eigenvalues of the  $2 \times 2$  matrix  $\Lambda(\omega)$ , see Eq. (49). These two relaxation lengths are depicted in Fig. 5.

In the large-frequency limit, we may approximate

$$\Lambda(\omega) \approx \frac{e^{i\pi/4}}{\sqrt{\omega}} \mathcal{C}_{\text{m}}^{-1/2} \Sigma_{\text{m}}^{1/2} \quad (78)$$

where  $\omega > 0$  and  $\Lambda(\omega) = \Lambda(-\omega)^*$ . Since the four entries of the response matrix  $\Sigma_{\text{m}}$  are all of comparable magnitude — all four entries are governed by the momentum relaxation time  $\tau_{\text{m}}$  —, the two relaxation lengths  $l_1(\omega) \sim (D_{\text{ex}} \tau_{\text{m}} k_B T / \hbar \omega)^{1/2}$  and  $l_2(\omega) \sim (D_{\text{ex}} \tau_{\text{m}} k_B T / \hbar \omega)^{1/2} (\hbar \omega_0 / k_B T)^{1/4}$  are determined by the two principal values of the response matrix  $\mathcal{C}_{\text{m}}$ , which

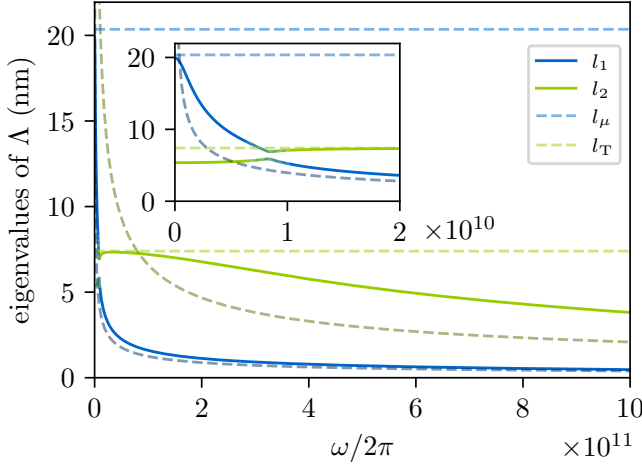


FIG. 5. Eigenvalues  $l_1$  and  $l_2$  of  $\Lambda$ , Eq. (49). The eigenvalues at zero frequency correspond to the characteristic decay lengths  $l_\mu$ , Eq. (80), and  $l_T$ , Eq. (81), for magnon or heat transport, respectively. Their numerical values are given in Tab. II. We refer to Sec. III E for an estimate of  $l_m(\omega)$ ,  $m = 1, 2$ , in the large-frequency limit.

differ by a factor  $\sim \sqrt{k_B T / \hbar \omega_0}$ , see App. A. As seen in Fig. 5, however, for the longer relaxation length the asymptotic frequency dependence sets in only for frequencies well above 1 THz.

If the frequency  $\omega$  is large enough that  $l_m(\omega) \ll d_F$ ,  $m = 1, 2$ , the effective impedances  $\mathcal{Z}_{ij\parallel}(\omega)$  become

$$\begin{aligned} \mathcal{Z}_{11\parallel}(\omega) &\approx \mathcal{Z}_{\text{FN}1\parallel} + \frac{e^{i\pi/4}}{\sqrt{\omega}} \mathcal{C}_m^{-1/2} \Sigma_m^{-1/2}, \\ \mathcal{Z}_{21\parallel}(\omega) &\approx \frac{e^{-i\pi/4} \sqrt{\omega}}{2} \mathcal{Z}_{\text{FN}1\parallel} \Sigma_m^{1/2} \mathcal{C}_m^{1/2} e^{\Lambda(\omega)^{-1} d_F} \mathcal{Z}_{\text{FN}2\parallel}, \end{aligned} \quad (79)$$

where  $\mathcal{Z}_{12\parallel}(\omega)$  and  $\mathcal{Z}_{22\parallel}(\omega)$  can be obtained by interchanging the labels  $1 \leftrightarrow 2$  and  $\mathcal{Z}_{ii\parallel}(\omega) = \mathcal{Z}_{ii\parallel}(-\omega)^*$ . The exponential increase of  $\mathcal{Z}_{21\parallel}(\omega)$  with  $d_F$  signals an exponential suppression of the longitudinal contribution to the nonlocal response with  $\sqrt{\omega}$  in the limit of large frequency  $\omega$ . For the material parameters of a Pt|YIG|Pt trilayer with  $d_F$  in the nm range, this means that the longitudinal contribution to the nonlocal conductivities becomes vanishingly small for  $\omega$  in the GHz range and above.

For the low-frequency limit of the longitudinal response, the relaxation lengths  $l_m(\omega)$  for magnon spin and energy density depend not only on the momentum relaxation time  $\tau_m$ , but also on the much longer relaxation times  $\tau_{\text{mp,ex}}$ ,  $\tau_{\text{mp,rel}}$ , and  $\tau_{\text{m,rel}}$ . Of these, relaxation by exchange-based magnon-phonon scattering is dominant at room temperature. Since exchange-based magnon-phonon scattering conserves the magnon spin density, but not the magnon energy density, the smallest relaxation length  $l_2(0) \sim l_T$  describes the relaxation of the magnon temperature, whereas the relaxation length  $l_1(0) \sim l_\mu$  for the magnon chemical potential is much larger. We define

$l_\mu$  and  $l_T$  based on Eq. (49), but omit off-diagonal matrix elements and neglect spin-Seebeck coupling in the approximation below (compare with Ref. 34),

$$\begin{aligned} l_\mu &\equiv ([\mathcal{G}_m^{-1}]_{s\mu} [\Sigma]_{s\mu})^{1/2} \\ &\approx \left( 2D_{\text{ex}} \tau_m \tau_{\text{rel}} \sqrt{\Delta k_B T \zeta(3/2) / \sqrt{\pi} \hbar} \right)^{1/2}, \end{aligned} \quad (80)$$

$$\begin{aligned} l_T &\equiv ([\mathcal{G}_m^{-1}]_{\text{QT}} [\Sigma]_{\text{QT}})^{1/2} \\ &\approx (4D_{\text{ex}} \tau_m \tau_{\text{mp,ex}} k_B T / \hbar)^{1/2}. \end{aligned} \quad (81)$$

Here,  $\tau_{\text{rel}} = \min(\tau_{\text{m,rel}}, \tau_{\text{mp,rel}})$  and the subscripts “s $\mu$ ” and “QT” point to the upper left and lower right matrix elements of the  $2 \times 2$  matrices, respectively. The values of  $l_\mu$  and  $l_T$  are shown in Tab. II and are close to the actual eigenvalues of  $\Lambda$ , see Fig. 5. In the limit of small thickness  $d_F \ll l_T (\ll l_\mu)$  of the ferromagnetic layer, the longitudinal impedances then become

$$\begin{aligned} \mathcal{Z}_{11\parallel}(0) &\approx \mathcal{Z}_{21\parallel}(0) \\ &\approx \mathcal{Z}_{\text{FN}1\parallel} + \mathcal{Z}_{\text{FN}2\parallel} + d_F \Sigma_m^{-1}(0). \end{aligned} \quad (82)$$

If  $l_T \ll d_F \ll l_\mu$ , no simple approximate expressions for the effective impedances can be derived. Since in this intermediate regime a nonequilibrium magnon distribution exists in the entire ferromagnetic layer, the order of magnitude of the nonlocal response is still that of Eq. (82), albeit with a different numerical prefactor. In the limit of large  $d_F$ , such that  $(l_T \ll) l_\mu \ll d_F$ , one finds

$$\begin{aligned} \mathcal{Z}_{11\parallel}(0) &\approx \mathcal{Z}_{\text{FN}1\parallel} + \mathcal{G}_m^{-1/2} \Sigma_m(0)^{-1/2} \\ \mathcal{Z}_{21\parallel}(0) &\approx \frac{1}{2} (\mathcal{Z}_{\text{FN}1\parallel} \mathcal{Z}_{\text{F}\parallel}^\infty(0)^{-1} + \mathbb{1}) e^{\Lambda(0)^{-1} d_F} \\ &\quad \times (\mathcal{Z}_{\text{FN}2\parallel} + \mathcal{Z}_{\text{F}\parallel}^\infty(0)), \end{aligned} \quad (83)$$

where

$$\mathcal{Z}_{\text{F}\parallel}^\infty(0) = \mathcal{G}_m^{-1/2} \Sigma_m^{-1/2} \quad (84)$$

is the zero-frequency spin impedance of the ferromagnet. For  $\mathcal{Z}_{21\parallel}(0)$ , this gives the order-of-magnitude estimate

$$\begin{aligned} \mathcal{Z}_{21\parallel}(0) &\sim \frac{2e^2 k_B T \sqrt{\tau_m}}{\hbar^2 D_{\text{ex}} \sqrt{\tau_{\text{rel}}}} \left( \mathcal{Z}_{\text{FN}1\parallel} + \frac{\hbar^2 D_{\text{ex}} \sqrt{\tau_{\text{rel}}}}{2e^2 k_B T \sqrt{\tau_m}} \right) \\ &\quad \times \left( \mathcal{Z}_{\text{FN}2\parallel} + \frac{\hbar^2 D_{\text{ex}} \sqrt{\tau_{\text{rel}}}}{2e^2 k_B T \sqrt{\tau_m}} \right) e^{d_F / l_\mu}, \end{aligned} \quad (85)$$

from which one easily derives an order-of-magnitude estimate for the nonlocal conductivities.

One of the key features of the spin-Hall magnetoresistance effect is that the electrical conductivity depends on the direction of the magnetization in F, as can be seen from Eqs. (66) and (67). Specifically, both  $\sigma_{ji}^{xx}$  and  $\sigma_{ji}^{yx}$  show a characteristic sine-like behavior with respect to the angle  $\theta$  between the magnetization direction and the  $y$ -axis. While  $\sigma_{ji}^{yx}$  changes sign for different angles  $\theta$ , the (correction to the) charge current in direction of the applied field,  $\sigma_{ji}^{xx}$ , is strictly negative for zero frequency

and therefore acts as an effective resistance in N1. For angles  $\theta = n\pi/2$  with  $n = 1, 3$  the conductivity (correction)  $\sigma_{ji}^{xx}(\omega = 0)$  vanishes and takes the highest absolute value for  $n = 0, 2$ . This means, an N|F|N trilayer or lateral device can act as a pure spin valve if it is possible to rotate the magnetization by  $\pi/2$ , *e.g.*, via an external magnetic field, and thereby switching the current in N2 on or off.

#### IV. BILINEAR RESPONSE

In this Section, we consider the quadratic-in-field contributions  $\bar{i}_j^{x,y}(t)^{(2)}$  to the spatially averaged charge current. The general relation for this bilinear response is of the form

$$\begin{aligned}\bar{i}_i^x(\Omega)^{(2)} &= \sum_{j,k=1}^2 \int \frac{d\omega}{2\pi} \sigma_{ijk}^{xxx(2)}(\omega_+, \omega_-) E_j(\omega_+) E_k(\omega_-)^*, \\ \bar{i}_i^y(\Omega)^{(2)} &= \sum_{j,k=1}^2 \int \frac{d\omega}{2\pi} \sigma_{ijk}^{yxx(2)}(\omega_+, \omega_-) E_j(\omega_+) E_k(\omega_-)^*,\end{aligned}\quad (86)$$

where  $\omega_{\pm} = \omega \pm \Omega/2$ . For an applied electric field at frequency  $\omega$ , Eq. (86) describes a current response at frequency  $\Omega = 0$  and at  $\Omega = 2\omega$ .

We calculate and compare the bilinear response coefficients  $\sigma_{ijk}^{xxx(2)}(\omega_+, \omega_-)$  and  $\sigma_{ijk}^{yxx(2)}(\omega_+, \omega_-)$  for three mechanisms: (i) The charge and spin currents heat up the normal metals N1 and N2 through Joule heating. Via the spin-Seebeck effect (SSE), the excess temperature in N1 and N2 drives a spin current through the F|N interfaces, which, via the inverse spin-Hall effect, leads to charge currents in N1 and N2. (ii) The longitudinal spin conductance of the ferromagnet–normal-metal interface has a nonlinear component, which gives a current response quadratic in the driving field. This contribution to the charge current is known as the magnonic unidirectional spin-Hall magnetoresistance (USMR) [40, 51]. (iii) Since longitudinal and transverse spin currents are defined with respect to the magnetization direction, a coherent precession of the magnetization itself causes a mixing of longitudinal and transverse responses, which also gives a current response bilinear in the applied field. Such a response is a current-in-plane version of the current-induced spin-torque diode effect (STD) [41, 42]. These three corrections are considered separately in Secs. IV A, IV B, and IV C. In Sec. IV D we numerically evaluate these results using parameter values for a Pt|YIG|Pt trilayer. We compare the three contributions to the nonlinear response and find their characteristic dependences on driving frequency  $\omega$  and the magnetization direction  $\mathbf{m}_{\text{eq}}$ . Additional details of the calculation can be found in App. B.

#### A. Bilinear SSE contribution

To describe the bilinear current response due to Joule heating and the SSE, we take Joule heating in Eq. (23) into account such that we arrive at a modified heat diffusion Equation (27),

$$\frac{\partial^2}{\partial z^2} \Delta u_{\text{eQ}}(z, \Omega) = \frac{\Delta u_{\text{eQ}}(z, \Omega)}{l_{\text{ep},i}(\Omega)^2} - \frac{k_{\text{B}} s(z, \Omega)}{e \kappa_{\text{ei}}}. \quad (87)$$

The Joule heating rate  $s(z, t)$  has contributions from charge and spin currents [75, 76], which for our geometry read

$$s(z, t) = E_i(t) i^x(z, t) - \frac{1}{2} \frac{\partial}{\partial z} (\mathbf{u}_s(z, t) \cdot \mathbf{i}_s^z(z, t)). \quad (88)$$

We here neglect corrections to the Joule heating from the spin-Hall effect and its inverse since they are proportional to the square of the spin-Hall angle and approximate

$$s_i(t) = \sigma_{\text{Ni}} E_i(t)^2 \quad (89)$$

for the normal layer Ni,  $i = 1, 2$ . (Complete expressions, which include the Joule heating from dissipative spin currents, are given in App. B and will be considered in the numerical evaluation in Sec. IV D.)

Solving Eqs. (26) and (87) for the heat currents  $i_{\text{Qi}}$  at the ferromagnet–normal-metal interfaces, with the boundary condition of vanishing heat currents at the insulator–normal-metal interfaces, gives

$$(-1)^{i-1} Z_{\text{QNi}}(\Omega) i_{\text{Qi}}(\Omega) = \Delta u_{\text{eQi}}(\Omega) - \delta u_{\text{eQi}}(\Omega), \quad (90)$$

with the source term

$$\begin{aligned}\delta u_{\text{eQ1}}(\Omega) &= \frac{2}{i_{\text{N1}}} \frac{l_{\text{ep1}}(\Omega)}{l_{\text{ep1}}(0)} \\ &\times \int_0^{d_{\text{N1}}} dz' s(z', \Omega) \frac{\cosh[(d_{\text{N1}} - z')/l_{\text{ep1}}(\Omega)]}{\sinh[d_{\text{N1}}/l_{\text{ep1}}(\Omega)]},\end{aligned}\quad (91)$$

where

$$i_{\text{Ni}} = \frac{2e}{k_{\text{B}}} \sqrt{\frac{\kappa_{\text{ei}} C_{\text{ei}}}{\tau_{\text{ep},i}}} \quad (92)$$

has the dimension of “charge current density” and serves as a characteristic current density for the nonlinear SSE response. We recall that  $l_{\text{ep}}$  is the thermal relaxation length defined in Eq. (28),  $\kappa_{\text{e}}$  is the thermal conductivity, and  $C_{\text{e}}$  the electronic heat capacity. The expression for  $\delta u_{\text{eQ2}}(\Omega)$  is analogous.

Inserting the approximation in Eq. (89) and performing a Fourier transform, the source terms  $\delta u_{\text{eQi}}(\Omega)$  become

$$\delta u_{\text{eQi}}(\Omega) = \frac{Z_{\text{Ni}}}{2\pi i_{\text{Ni}}} \frac{l_{\text{ep},i}(\Omega)^2}{l_{\text{ep},i}(0) \lambda_{\text{Ni}}} \sigma_{\text{Ni}}^2 \int d\omega E_i(\omega_+) E_i(-\omega_-), \quad (93)$$

where  $\omega_{\pm} = \omega \pm \Omega/2$  and the spin impedance  $Z_{Ni}$  was defined in Eq. (22).

To find the bilinear response at frequency  $\Omega$ , we calculate the longitudinal spin current densities and the heat current densities from Eqs. (21), (33), (54), and (90), where we replace  $\omega$  by  $\Omega$  and set the driving field in

Eq. (21) to zero,

$$\begin{pmatrix} i_{si\parallel}(\Omega)^{(2)} \\ i_{Qi}(\Omega)^{(2)} \end{pmatrix} = - \sum_{j=1}^2 \mathcal{Z}_{ij}^{-1}(\Omega) (-1)^{j-1} \begin{pmatrix} 0 \\ \delta u_{eQi}(\Omega) \end{pmatrix}. \quad (94)$$

The quadratic-in- $E$  charge current densities can then be calculated from the inverse spin-Hall effect,

$$\begin{aligned} i_i^x(\Omega)^{(2)} &= \frac{\lambda_{Ni}}{d_{Ni}} \theta_{SHi} \left[ i_{si\parallel}(\Omega)^{(2)} \mathbf{e}_y \cdot \mathbf{m}_{eq} + i_{si\perp}(\Omega)^{(2)} \mathbf{e}_y \cdot \mathbf{e}_{\perp} + i_{si\perp}(-\Omega)^{(2)*} \mathbf{e}_y \cdot \mathbf{e}_{\perp}^* \right], \\ i_i^y(\Omega)^{(2)} &= - \frac{\lambda_{Ni}}{d_{Ni}} \theta_{SHi} \left[ i_{si\parallel}(\Omega)^{(2)} \mathbf{e}_x \cdot \mathbf{m}_{eq} + i_{si\perp}(\Omega)^{(2)} \mathbf{e}_x \cdot \mathbf{e}_{\perp} + i_{si\perp}(-\Omega)^{(2)*} \mathbf{e}_x \cdot \mathbf{e}_{\perp}^* \right]. \end{aligned} \quad (95)$$

Combining Eqs. (93), (94), and (95), we find that the charge current associated with Joule heating is of the form (86), with

$$\sigma_{ijk}^{xxx(2)}(\omega_+, \omega_-)_{\text{Joule}} = \frac{\lambda_{Ni}}{d_{Ni} i_{Ni}} \sigma_{Nj} \sigma_{Nk} \left[ v_{ijk}(\omega_+, \omega_-) m_y + v'_{ijk}(\omega_+, \omega_-) m_y (1 - m_y^2) \right], \quad (96)$$

$$\sigma_{ijk}^{xxx(2)}(\omega_+, \omega_-)_{\text{Joule}} = - \frac{\lambda_{Ni}}{d_{Ni} i_{Ni}} \sigma_{Nj} \sigma_{Nk} \left[ v_{ijk}(\omega_+, \omega_-) m_x + v'_{ijk}(\omega_+, \omega_-) m_x (1 - m_y^2) \right]. \quad (97)$$

The dimensionless response coefficients  $v_{ijk}$  in Eqs. (96) and (97) read

$$v_{ijk}(\omega_+, \omega_-) = - \theta_{SHi} \chi_{ij}(\Omega) (-1)^{j-1} \frac{l_{ep,j}(\Omega)^2}{l_{ep,j}(0) \lambda_{Nj}} \delta_{jk}, \quad (98)$$

where

$$\chi_{ji}(\omega) = Z_{Ni} \left[ \mathcal{Z}_{ji}^{-1}(\omega) \right]_{sT}. \quad (99)$$

The indices “s” and “T” in Eq. (99) refer to the  $2 \times 2$  matrix structure introduced in Eqs. (33) and (34) and denote a spin current response to a temperature difference. These bilinear response coefficients represent the SSE contribution from Joule heating by dissipative charge currents in N. The dimensionless bilinear response coefficients  $v'_{ijk}(\omega_+, \omega_-)$  arise from the Joule heating of dissipative spin currents, which is not contained in the approximation (89). An expression for these coefficients can be found in App. B.

The characteristic current density  $i_{Ni}$  describes at which linear-response current  $i_i^{(1)} = \sigma_{Ni} E_i$  the nonlinear current response  $i_i^{(2)}$  is of the of the same order as  $i_i^{(1)}$  — up to a numerical factor, which is the product of the geometry-dependent ratio  $\lambda_{Ni}/d_{Ni}$  and the coefficients  $v_{ijk}$  and  $v'_{ijk}$  in Eqs. (96) and (97). As will be shown in Sec. IV D, for typical material parameters, the factors  $v_{ijk}$  and  $v'_{ijk}$  are numerically small — of order  $10^{-2}$  and below —, because of the numerical smallness of the spin-Hall angle  $\theta_{SHi}$  and of the impedance ratio

$\chi_{ji}$ . (The smallness of the impedance ratio  $\chi_{ji}$  reflects a spin impedance mismatch at a typical F|N interface.) Since the SSE contribution dominates the nonlinear response at low frequencies, we will also use the characteristic current density  $i_{Ni}$  as a reference current density for the nonlinear responses from the nonlinearity of the longitudinal interfacial spin conductance (USMR, Sec. IV B) and from the coherent precession of the magnetization (STD, Sec. IV C).

## B. Bilinear USMR contribution

In Sec. III B we accounted for the spin and heat currents through the ferromagnet–normal-metal interfaces to linear order in the (generalized) potential differences  $u_{si} - u_{mi}$  and  $u_{eQi} - u_{mQi}$ . Following Ref. 51, we now include second-order contributions to the interfacial spin and heat currents.

The interfacial boundary condition, Eq. (33), has a correction quadratic in the current densities  $i_{si\parallel}$ ,  $i_{Qi}$ , the spin accumulation  $u_{si\parallel}$ , and the electronic excess temperature  $\Delta u_{eQi}$ ,

$$\begin{aligned} \begin{pmatrix} u_{si\parallel} - u_{mi} \\ \Delta u_{eQi} - \Delta u_{mQi} \end{pmatrix} &= - (-1)^{i-1} \mathcal{Z}_{FNi\parallel} \\ &\times \left[ \begin{pmatrix} i_{si\parallel} \\ i_{Qi} \end{pmatrix} + \begin{pmatrix} \delta i_{si\parallel} \\ \delta i_{Qi} \end{pmatrix} \right], \end{aligned} \quad (100)$$

where the corrections to the current densities are of the



form (using a  $2 \times 2$  matrix notation)

$$\begin{aligned}\delta i_{si\parallel}(t) &= \frac{1}{i_{\text{FN}i}} \left[ (-1)^{i-1} \begin{pmatrix} u_{si\parallel}(t) & \Delta u_{eQ_i}(t) \end{pmatrix} \mathcal{A}_{si} \begin{pmatrix} i_{si\parallel}(t) \\ i_{Qi}(t) \end{pmatrix} \right. \\ &\quad \left. + \begin{pmatrix} i_{si\parallel}(t) & i_{Qi}(t) \end{pmatrix} \mathcal{B}_s \begin{pmatrix} i_{si\parallel}(t) \\ i_{Qi}(t) \end{pmatrix} \right], \\ \delta i_{Qi}(t) &= \frac{1}{i_{\text{FN}i}} \left[ (-1)^{i-1} \begin{pmatrix} u_{si\parallel}(t) & \Delta u_{eQ_i}(t) \end{pmatrix} \mathcal{A}_{Qi} \begin{pmatrix} i_{si\parallel}(t) \\ i_{Qi}(t) \end{pmatrix} \right. \\ &\quad \left. + \begin{pmatrix} i_{si\parallel}(t) & i_{Qi}(t) \end{pmatrix} \mathcal{B}_Q \begin{pmatrix} i_{si\parallel}(t) \\ i_{Qi}(t) \end{pmatrix} \right].\end{aligned}\quad (101)$$

Here, the characteristic interfacial current density

$$i_{\text{FN}i} = \frac{3\text{Re}(g_{\uparrow\downarrow i})}{4\pi^{3/2}eS} k_T^3 k_B T, \quad (102)$$

with  $k_T$  defined in Eq. (35) and the spin density  $s$ , describes the ferromagnet–normal-metal interface. The

nonlinear response matrices  $\mathcal{A}_{si}$ ,  $\mathcal{A}_{Qi}$ ,  $\mathcal{B}_s$  and  $\mathcal{B}_Q$  can be calculated as in the linearized case [34] to leading order in the spin-mixing conductance  $g_{\uparrow\downarrow}$  [77], but higher orders in spin accumulation, magnon chemical potential, and electron and magnon temperatures. Detailed expressions are presented in App. B.

Since the generalized potentials  $u_{si\parallel}$  and  $\Delta u_{eQ_i}$  and the current densities  $i_{si\parallel}$  and  $i_{Qi}$  are known to first order in the electric field, see Sec. III, we may also obtain expressions for the second-order-in- $E_i$  source terms  $\delta i_{si\parallel}$  and  $\delta i_{Qi}$ . We then calculate the longitudinal spin current densities and the heat current densities from Eqs. (21), (54), and (100),

$$\begin{pmatrix} i_{si\parallel}(\Omega)^{(2)} \\ i_{Qi}(\Omega)^{(2)} \end{pmatrix} = \sum_{j=1}^2 \mathcal{Z}_{ij\parallel}^{-1}(\Omega) \mathcal{Z}_{\text{FN}j\parallel} \begin{pmatrix} \delta i_{sj\parallel}(\Omega) \\ \delta i_{Qj}(\Omega) \end{pmatrix}. \quad (103)$$

For the bilinear charge current response due to the magnonic USMR we then find

$$\sigma_{ijk}^{xx(2)}(\omega_+, \omega_-)_{\text{USMR}} = \frac{\lambda_{Ni}}{d_{Ni}i_{Ni}} \sigma_{Nj} \sigma_{Nk} r_{ijk}(\omega_+, \omega_-) m_y^3, \quad (104)$$

$$\sigma_{ijk}^{yx(2)}(\omega_+, \omega_-)_{\text{USMR}} = - \frac{\lambda_{Ni}}{d_{Ni}i_{Ni}} \sigma_{Nj} \sigma_{Nk} r_{ijk}(\omega_+, \omega_-) m_x m_y^2, \quad (105)$$

where the dimensionless coefficient  $r_{ijk}$  is given by (using  $2 \times 2$  matrix notation)

$$\begin{aligned}r_{ijk}(\omega_+, \omega_-) &= \theta_{\text{SH}i} \theta_{\text{SH}j} \theta_{\text{SH}k} \frac{i_{Ni}}{i_{\text{FN}i}} \sum_{l=1}^2 \sum_{\alpha=\mu, T} \left[ \mathcal{Z}_{il\parallel}^{-1}(\Omega) \mathcal{Z}_{\text{FN}l\parallel} \right]_{s\alpha} \\ &\quad \times \left[ (-Z_{Ni}[\delta_{lj} - \zeta_{lj\parallel}(\omega_+)] \Phi_{lj}(\omega_+) Z_{Nj}) \mathcal{A}_{\alpha l} \begin{pmatrix} \zeta_{lk\parallel}(\omega_-) \\ \phi_{lk}(\omega_-) \end{pmatrix} + (\zeta_{lj\parallel}(\omega_+) \phi_{lj}(\omega_+)) \mathcal{B}_{\alpha} \begin{pmatrix} \zeta_{lk\parallel}(\omega_-) \\ \phi_{lk}(\omega_-) \end{pmatrix} \right],\end{aligned}\quad (106)$$

with  $\mathcal{Z}_{il\parallel}(\omega)$  defined in Eqs. (61) and (62). To facilitate a comparison with the Joule-heating contribution to the charge currents, we have used the Joule-heating characteristic current density  $i_{Ni}$  as reference current density in Eqs. (104) and (105).

### C. Bilinear STD contribution

The longitudinal and transverse components of the spin current and of the spin accumulation are defined with respect to the magnetization axis. Because the magnetization direction  $\mathbf{m}$  itself is time dependent, the current-driven magnetization precession leads to a charge current response quadratic in the driving field [48, 78], analogous to the current-induced spin-torque diode effect (STD) [41, 42]. A theory for this effect was previously formulated by Chiba, Bauer, and Takahashi [48] for a F|N bilayer in the macrospin approximation and with-

out accounting for longitudinal spin currents and heat transport across the interface. Building on the analysis of Ref. 48, we here calculate the local and nonlocal spin-torque diode contributions to the charge currents taking into account coherent as well as incoherent magnon transport in F.

In the linear response theory of Sec. III, we have used the equilibrium magnetization direction  $\mathbf{m}_{\text{eq}}$  as the reference direction to define longitudinal and transverse spin currents. For the response bilinear in the driving field, the deviations of  $\mathbf{m}$  from the equilibrium direction  $\mathbf{m}_{\text{eq}}$  must be taken into account when defining the longitudinal and transverse contributions. Hereto, we replace the basis  $\{\mathbf{m}_{\text{eq}}, \mathbf{e}_{\perp}, \mathbf{e}_{\perp}^*\}$  of Eqs. (6)–(8) by the basis  $\{\mathbf{m}_i(t), \tilde{\mathbf{e}}_{\perp i}(t), \tilde{\mathbf{e}}_{\perp i}(t)^*\}$ , where  $\mathbf{m}_i(t)$  is the magnetization direction at the interface with Ni,  $i = 1, 2$ , and the complex unit vector  $\tilde{\mathbf{e}}_{\perp i}(t)$  satisfies the time-dependent version of Eq. (7),  $\tilde{\mathbf{e}}_{\perp i}(t) \times \mathbf{m}(t) = i \tilde{\mathbf{e}}_{\perp i}(t)$ . To first order

in the magnetization amplitude  $m_{\perp i}(t)$  one has

$$\begin{aligned}\mathbf{m}_i(t) &= \mathbf{m}_{\text{eq}} + 2\text{Re } m_{\perp i}(t) \mathbf{e}_{\perp}, \\ \tilde{\mathbf{e}}_{\perp i}(t) &= \mathbf{e}_{\perp} - m_{\perp i}^*(t) \mathbf{m}_{\text{eq}}.\end{aligned}\quad (107)$$

The longitudinal and transverse spin currents through the F|N interfaces depend on the longitudinal and transverse components of the spin accumulation in N, which must be calculated relative to the basis vectors  $\mathbf{m}(t)$  and  $\tilde{\mathbf{e}}_{\perp}(t)$ , respectively. From Eq. (107) we then find

$$\begin{aligned}\tilde{u}_{s\parallel}(t) &= u_{\parallel i}(t) + 2\text{Re } m_{\perp i}^*(t) u_{s\perp}(t), \\ \tilde{u}_{s\perp}(t) &= u_{\perp i}(t) - m_{\perp i}(t) u_{s\parallel}(t),\end{aligned}\quad (108)$$

where  $u_{s\parallel}(t)$  and  $u_{s\perp}(t)$  are the longitudinal and transverse components of  $\mathbf{u}_s(t)$  defined with respect to the equilibrium magnetization direction  $\mathbf{m}_{\text{eq}}$ . Longitudinal and transverse components  $\tilde{i}_{s\parallel}(t)$  and  $\tilde{i}_{s\perp}(t)$  of the spin currents at the interfaces, defined with respect to the  $\mathbf{m}_i(t)$ -dependent basis vectors at the interfaces, can then be calculated from the linear response theory of the previous sections, replacing  $u_{s\parallel}(t)$  and  $u_{s\perp}(t)$  by  $\tilde{u}_{s\parallel}(t)$  and  $\tilde{u}_{s\perp}(t)$ , respectively,

$$\begin{aligned}\begin{pmatrix} \tilde{i}_{s\parallel}(t) \\ \tilde{i}_{Q_i}(t) \end{pmatrix} &= -(-1)^{i-1} Z_{\text{FN}i\parallel}^{-1} \begin{pmatrix} \tilde{u}_{s\parallel}(t) - u_{\text{m}i}(t) \\ u_{\text{e}Q_i}(t) - u_{\text{m}Q_i}(t) \end{pmatrix}, \\ \tilde{i}_{s\perp}(t) &= -(-1)^{i-1} \frac{1}{Z_{\text{FN}i\perp}} (\tilde{u}_{s\perp}(t) + i(\hbar/e) \dot{m}_{\perp i}(t)),\end{aligned}\quad (109)$$

(Compare with Eqs. (31) and (33).) We express the relation

$$\mathbf{i}_{si}(t) = \tilde{i}_{s\parallel}(t) \mathbf{m}_i(t) + 2\text{Re } \tilde{i}_{s\perp}(t) \tilde{\mathbf{e}}_{\perp i}(t) \quad (110)$$

in terms of its longitudinal and transverse components defined with respect to the time-independent basis vec-

tors  $\mathbf{m}_{\text{eq}}$  and  $\mathbf{e}_{\perp}$  and obtain

$$\begin{aligned}i_{s\parallel}(t) &= \tilde{i}_{s\parallel}(t) - 2\text{Re } m_{\perp i}^*(t) \tilde{i}_{s\perp}(t), \\ i_{s\perp}(t) &= \tilde{i}_{s\perp}(t) + m_{\perp i}(t) \tilde{i}_{s\parallel}(t).\end{aligned}\quad (111)$$

These equations can be used as the starting point to calculate the spin currents through the F|N interfaces to second order in the driving fields  $E_i(t)$ ,  $i = 1, 2$ . For longitudinal spin transport and for heat transport across the interface we find, after a Fourier transform to frequency, an interface relation of the same form as Eq. (100), but with source terms

$$\begin{aligned}\begin{pmatrix} \delta i_{s\parallel}(t) \\ \delta i_{Q_i}(t) \end{pmatrix} &= -(-1)^{i-1} Z_{\text{FN}i\parallel}^{-1} \begin{pmatrix} 2\text{Re } m_{\perp i}^*(t) u_{s\perp}(t) \\ 0 \end{pmatrix} \\ &\quad - \begin{pmatrix} 2\text{Re } m_{\perp i}^*(t) i_{s\perp}(t) \\ 0 \end{pmatrix}.\end{aligned}\quad (112)$$

For the transverse component we find

$$\begin{aligned}u_{s\perp}(\Omega) + (\hbar\Omega/e) m_{\perp i}(\Omega) \\ = -(-1)^{i-1} Z_{\text{FN}i\perp} (i_{s\perp}(\Omega) + \delta i_{s\perp}(\Omega))\end{aligned}\quad (113)$$

with

$$\delta i_{s\perp}(t) = (-1)^{i-1} \frac{m_{\perp i}(t) u_{s\parallel}(t)}{Z_{\text{FN}i\perp}} + m_{\perp i}(t) i_{s\parallel}(t). \quad (114)$$

Since they are quadratic in the applied field, the source terms  $\delta i_{s\parallel}$ ,  $\delta i_{Q_i}$ , and  $\delta i_{s\perp}$  may be calculated from the linear-response theory of Sec. III. The explicit expressions are given in App. B.

The transverse component of the second-order spin current is calculated from Eqs. (21), (40) and (113), where we replace  $\omega$  by  $\Omega$  in Eqs. (21) and (40) and set the driving field in Eq. (21) to zero. This gives

$$i_{s\perp}(\Omega)^{(2)} = \sum_{j=1}^2 \frac{Z_{\text{FN}j\perp}}{Z_{ij\perp}(\Omega)} \delta i_{sj\perp}(\Omega), \quad (115)$$

whereas the longitudinal component is given by Eq. (103). Combining everything, we find that the quadratic-in-field STD contribution to the charge current is

$$\sigma_{ijk}^{xxx(2)}(\omega_+, \omega_-)_{\text{STD}} = \frac{\lambda_{Ni}}{d_{Ni} i_{Ni}} \sigma_{Nj} \sigma_{Nk} w'_{ijk}(\omega_+, \omega_-) m_y (1 - m_y^2), \quad (116)$$

$$\sigma_{ijk}^{yxx(2)}(\omega_+, \omega_-)_{\text{STD}} = -\frac{\lambda_{Ni}}{d_{Ni} i_{Ni}} \sigma_{Nj} \sigma_{Nk} [w_{ijk}(\omega_+, \omega_-) m_x + w''_{ijk}(\omega_+, \omega_-) m_z + w'_{ijk}(\omega_+, \omega_-) m_x (1 - m_y^2)], \quad (117)$$

where we again used the characteristic current density  $i_{Ni}$  of Eq. (92) as a reference. The dimensionless response

coefficients read

$$\begin{aligned}
w_{ijk}(\omega_+, \omega_-) &= \frac{1}{2} \theta_{\text{SH}i} \theta_{\text{SH}j} \theta_{\text{SH}k} \frac{i_{\text{Ni}}}{i_{\text{F}}} \sum_{l=1}^2 (-1)^{j-1} \\
&\quad \times \{ (-1)^{l+k} [\zeta_{il\perp}(\Omega) \eta_{j\perp}(\omega_+) (\delta_{lk} - \zeta_{lk\parallel}(\omega_-)^*) + \zeta_{il\perp}(-\Omega)^* \eta_{j\perp}(-\omega_+)^* (\delta_{lk} - \zeta_{lk\parallel}(-\omega_-))] \\
&\quad + \psi_{il\perp}(\Omega) \eta_{j\perp}(\omega_+) \zeta_{lk\parallel}(\omega_-)^* + \psi_{il\perp}(-\Omega)^* \eta_{j\perp}(-\omega_+)^* \zeta_{lk\parallel}(-\omega_-) \}, \\
w'_{ijk}(\omega_+, \omega_-) &= \frac{1}{2} \theta_{\text{SH}i} \theta_{\text{SH}j} \theta_{\text{SH}k} \frac{i_{\text{Ni}}}{i_{\text{F}}} \sum_{l=1}^2 (-1)^{j-1} \\
&\quad \times \{ (-1)^{l+k} \zeta_{il\parallel}(\Omega) [\eta_{j\perp}(-\omega_+)^* (\delta_{lk} - \zeta_{lk\perp}(-\omega_-)) + \eta_{j\perp}(\omega_+) (\delta_{lk} - \zeta_{lk\perp}(\omega_-)^*)] \\
&\quad - (-1)^{l+k} \zeta_{il\perp}(\Omega) \eta_{j\perp}(\omega_+) (\delta_{lk} - \zeta_{lk\parallel}(\omega_-)^*) \\
&\quad - (-1)^{l+k} \zeta_{il\perp}(-\Omega)^* \eta_{j\perp}(-\omega_+)^* (\delta_{lk} - \zeta_{lk\parallel}(-\omega_-)) \\
&\quad - \psi_{il\parallel}(\Omega) [\eta_{j\perp}(-\omega_+)^* \zeta_{lk\perp}(-\omega_-) + \eta_{j\perp}(\omega_+) \zeta_{lk\perp}(\omega_-)^*] \\
&\quad - \psi_{il\perp}(\Omega) \eta_{j\perp}(\omega_+) \zeta_{lk\parallel}(\omega_-)^* - \psi_{il\perp}(-\Omega)^* \eta_{j\perp}(-\omega_+)^* \zeta_{lk\parallel}(-\omega_-) \}, \\
w''_{ijk}(\omega_+, \omega_-) &= \frac{i}{2} \theta_{\text{SH}i} \theta_{\text{SH}j} \theta_{\text{SH}k} \frac{i_{\text{Ni}}}{i_{\text{F}}} \sum_{l=1}^2 (-1)^{j-1} \\
&\quad \times \{ (-1)^{l+k} [\zeta_{il\perp}(\Omega) \eta_{j\perp}(\omega_+) (\delta_{lk} - \zeta_{lk\parallel}(\omega_-)^*) - \zeta_{il\perp}(-\Omega)^* \eta_{j\perp}(-\omega_+)^* (\delta_{lk} - \zeta_{lk\parallel}(-\omega_-))] \\
&\quad + \psi_{il\perp}(\Omega) \eta_{j\perp}(\omega_+) \zeta_{lk\parallel}(\omega_-)^* - \psi_{il\perp}(-\Omega)^* \eta_{j\perp}(-\omega_+)^* \zeta_{lk\parallel}(-\omega_-) \}.
\end{aligned} \tag{118}$$

Here  $i_{\text{F}}$  was defined in Eq. (72),  $\zeta_{ji\perp}(\omega)$ ,  $\zeta_{ji\parallel}(\omega)$ , and  $\eta_{ji\perp}(\omega)$  are impedance ratios, defined in Eqs. (64), (65), and (75), respectively, and

$$\psi_{ji\perp}(\omega) = Z_{\text{FN}i\perp} / Z_{ji\perp}(\omega), \tag{119}$$

$$\psi_{ji\parallel}(\omega) = \left[ \mathcal{Z}_{ji\parallel}^{-1}(\omega) \mathcal{Z}_{\text{FN}i\parallel} \right]_{\text{s}\mu}. \tag{120}$$

#### D. Numerical estimates and discussion

Together, Eqs. (96), (97), (104), (105), (116), and (117) define the coefficients for the full bilinear response,

$$\begin{aligned}
\sigma_{ijk}^{xxx(2)} &= \sigma_{ijk, \text{Joule}}^{xxx(2)} + \sigma_{ijk, \text{USMR}}^{xxx(2)} + \sigma_{ijk, \text{STD}}^{xxx(2)}, \\
\sigma_{ijk}^{yxx(2)} &= \sigma_{ijk, \text{Joule}}^{yxx(2)} + \sigma_{ijk, \text{USMR}}^{yxx(2)} + \sigma_{ijk, \text{STD}}^{yxx(2)}.
\end{aligned} \tag{121}$$

Each of the partial response coefficients derived in the previous subsections has the same structure: It contains the geometry-dependent ratio  $\lambda_{\text{Ni}}/d_{\text{Ni}}$ , the product of bulk conductivities  $\sigma_{\text{N}j}\sigma_{\text{N}k}$ , the reference current density  $i_{\text{Ni}}$  of Eq. (92), and dimensionless coefficients  $v_{ijk}$ ,  $v'_{ijk}$ ,  $r_{ijk}$ ,  $w_{ijk}$ ,  $w'_{ijk}$ , and  $w''_{ijk}$ , which each multiply a characteristic dependence on the magnetization direction  $\mathbf{m}_{\text{eq}}$ . Since the differences between the three nonlinear current contributions are contained in the dimensionless coefficients, we focus on these in the remaining discussion.

To illustrate the quadratic response, we consider a harmonic driving field in N1,

$$E_1(t) = 2E \cos(\omega t), \tag{122}$$

so that

$$E_1(\omega') = 2\pi E [\delta(\omega' - \omega) + \delta(\omega' + \omega)], \tag{123}$$

whereas  $E_2(\omega') = 0$ . The quadratic-in- $E$  current response has components at frequencies  $\Omega = 0$  and  $\Omega = 2\omega$ ,

$$\bar{i}_i^x(t)^{(2)} = A_i^x E^2 + \text{Re } B_i^x E^2 e^{-2i\omega t}, \tag{124}$$

$$\bar{i}_i^y(t)^{(2)} = A_i^y E^2 + \text{Re } B_i^y E^2 e^{-2i\omega t}, \tag{125}$$

with real response coefficient  $A_i^{x/y} = \sigma_{i11}^{x/yxx(2)}(\omega, \omega) + \sigma_{i11}^{xxx(2)}(-\omega, -\omega)$  and complex response coefficient  $B_i^{x/y} = 2\sigma_{i11}^{x/yxx(2)}(\omega, -\omega)$ . From Eqs. (96), (97), (104), (105), (116), and (117), we find

$$\begin{aligned}
A_i^x &= \frac{\lambda_{\text{Ni}} \sigma_{\text{N}1}^2}{d_{\text{Ni}} i_{\text{Ni}}} \{ [v_{i11}^{\text{dc}} + r_{i11}^{\text{dc}}] m_y \\
&\quad + [v_{i11}'^{\text{dc}} - r_{i11}^{\text{dc}} + w_{i11}'^{\text{dc}}] m_y (1 - m_y^2) \},
\end{aligned} \tag{126}$$

$$\begin{aligned}
A_i^y &= - \frac{\lambda_{\text{Ni}} \sigma_{\text{N}1}^2}{d_{\text{Ni}} i_{\text{Ni}}} \{ [v_{i11}^{\text{dc}} + r_{i11}^{\text{dc}} + w_{i11}^{\text{dc}}] m_x \\
&\quad + [v_{i11}'^{\text{dc}} - r_{i11}^{\text{dc}} + w_{i11}'^{\text{dc}}] m_x (1 - m_y^2) + w_{i11}''^{\text{dc}} m_z \},
\end{aligned} \tag{127}$$

$$\begin{aligned}
B_i^x &= \frac{\lambda_{\text{Ni}} \sigma_{\text{N}1}^2}{d_{\text{Ni}} i_{\text{Ni}}} \{ [v_{i11}^{\text{ac}} + r_{i11}^{\text{ac}}] m_y \\
&\quad + [v_{i11}'^{\text{ac}} - r_{i11}^{\text{ac}} + w_{i11}'^{\text{ac}}] m_y (1 - m_y^2) \},
\end{aligned} \tag{128}$$

$$\begin{aligned}
B_i^y &= - \frac{\lambda_{\text{Ni}} \sigma_{\text{N}1}^2}{d_{\text{Ni}} i_{\text{Ni}}} \{ [v_{i11}^{\text{ac}} + r_{i11}^{\text{ac}} + w_{i11}^{\text{ac}}] m_x \\
&\quad + [v_{i11}'^{\text{ac}} - r_{i11}^{\text{ac}} + w_{i11}'^{\text{ac}}] m_x (1 - m_y^2) + w_{i11}''^{\text{ac}} m_z \},
\end{aligned} \tag{129}$$

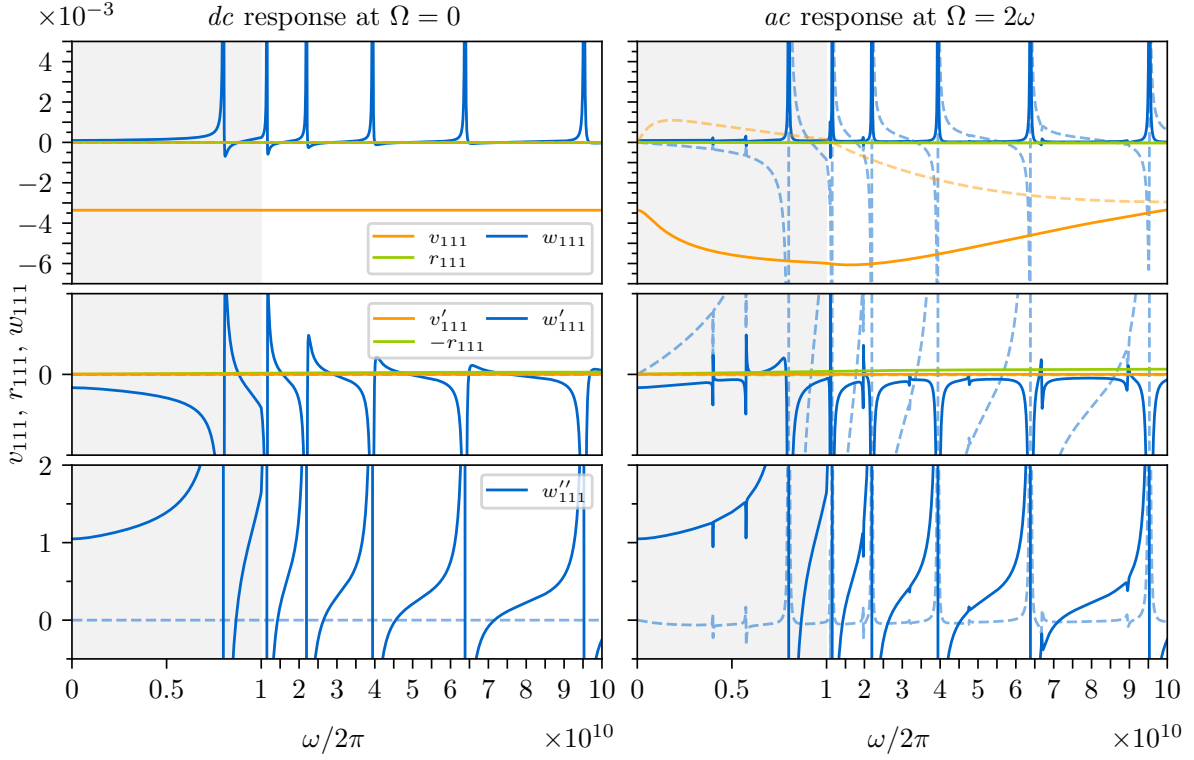


FIG. 6. Local nonlinear response coefficients  $v_{111}$  and  $v'_{111}$  from Joule heating,  $r_{111}$  and  $r'_{111}$  from USMR, and  $w_{111}$ ,  $w'_{111}$ , and  $w''_{111}$  from STD, see Eqs. (98), (106), and (118), respectively. These coefficients are proportional to the quadratic-in- $E$  charge current in N1, see Eqs. (124) and (125). The upper panels show contributions that scale linearly with an in-plane magnetization direction  $m_{x/y}$  of F, the primed coefficients in the middle panels are proportional to  $m_{x/y}(1 - m_y^2)$ , and the lower panels correspond to a charge current proportional to  $m_z$ . Solid curves denote real parts; dashed curves denote imaginary parts. Device and parameter values are taken from Tabs. I and II.

where we abbreviated

$$v_{i11}^{\text{dc}} = v_{i11}(\omega, \omega) + v_{i11}(-\omega, -\omega), \quad (130)$$

$$v_{i11}^{\text{ac}} = 2v_{i11}(\omega, -\omega), \quad (131)$$

and similarly for the other dimensionless coefficients. All contributions to the bilinear response change sign under a reversal of the magnetization direction, which is reminiscent of a unidirectional magnetoresistance (UMR) in bilayer systems. The in-plane magnetic-field dependence of the longitudinal response is consistent with that of the phenomenological theory of Ref. 38 and with the experimental observations in Refs. 40 and 79.

From Eqs. (126)–(129) we conclude that there is no bilinear response in the  $x$ -direction, *i.e.*, in the direction of the applied electric field, if the magnetization  $\mathbf{m}_{\text{eq}}$  in F is in the  $xz$ -plane, whereas the bilinear response in the  $y$ -direction disappears if  $\mathbf{m}_{\text{eq}}$  is in the  $y$ -direction.

For a comparison of the three contributions to the nonlinear response in a Pt|YIG|Pt trilayer, we consider the dimensionless coefficients  $v_{i11}$ ,  $v'_{i11}$ ,  $r_{i11}$ ,  $w_{i11}$ ,  $w'_{i11}$ , and  $w''_{i11}$ , as they appear in Eqs. (126)–(129) for the *dc* and *ac* response. In Figs. 6 and 7 we show these coefficients for local transport ( $i = 1$ ) and nonlocal transport ( $i = 2$ ),

respectively, as a function of the driving frequency  $\omega$  for the material parameters given in Tabs. I and II.

The nonlinear SSE, STD, and USMR effects can be distinguished via their dependence on the magnetization direction  $\mathbf{m}_{\text{eq}}$ , the driving frequency  $\omega$ , the strength of the external magnetic field, which enters into the theory via the ferromagnetic resonance frequency  $\omega_0$ , and the thickness  $d_F$  of the ferromagnetic layer. The dependence on the magnetization direction can be inferred directly from Eqs. (126)–(129) and the frequency dependence is illustrated in Figs. 6 and 7, whereas the dependence on the ferromagnetic resonance frequency  $\omega_0$  and the thickness  $d_F$  in the limit of low driving frequency  $\omega$  is illustrated in Figs. 8 and 9, respectively.

The SSE contribution from Joule heating by dissipative charge currents (response coefficients  $v_{i11}$ ,  $i = 1, 2$ ) and the USMR contribution to the bilinear response (response coefficients  $r_{i11}$ ) involve incoherent (thermal) magnons only. Correspondingly, these are smooth functions of the driving frequency  $\omega$ . The SSE contribution from Joule heating by dissipative spin currents (response coefficients  $v'_{i11}$ ) and the STD contributions to the bilinear response (response coefficients  $w_{i11}$ ,  $w'_{i11}$ , and  $w''_{i11}$ ) involve both coherent and incoherent magnons. These

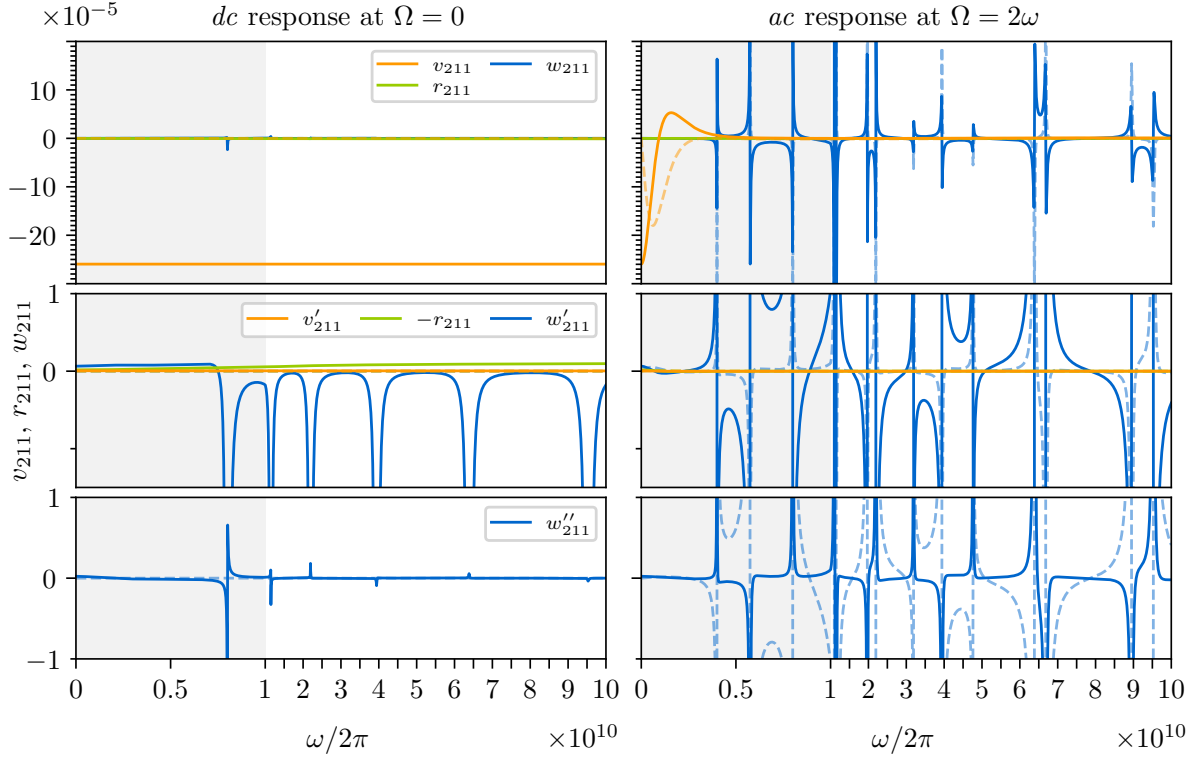


FIG. 7. Same as Fig. 6, but for the nonlocal nonlinear response coefficients, which describe the quadratic-in- $E$  charge current in N2 for an applied harmonic  $E(t)$ -field in N1.

terms show sharp features as a function of the driving frequency  $\omega$  if  $\omega$  equals a resonance frequency  $\omega_n$  or if  $\omega = \omega_n/2$ , whereby for the local response the resonant features at  $\omega = \omega_n/2$  are weaker than those at  $\omega = \omega_n$ , see Fig. 6.

In general, the SSE contribution from dissipative spin currents and the USMR contribution are much smaller than the SSE contribution from dissipative charge currents and the STD contribution. Which of the latter two dominates the bilinear response depends on the thickness  $d_F$  of the ferromagnetic layer, the ferromagnetic resonance frequency  $\omega_0$ , and whether the magnetization direction  $\mathbf{m}_{\text{eq}}$  is in-plane ( $m_z = 0$ ) or has an out-of-plane component ( $m_z \neq 0$ ). Away from the resonance frequencies, the  $xx$  bilinear response for all  $\mathbf{m}_{\text{eq}}$  and the  $xy$  response for  $m_z = 0$  are dominated by the SSE contribution  $v_{i11}$  from Joule heating by dissipative charge currents, except at very small  $d_F$  and  $\omega_0$  ( $d_F \lesssim 10$  nm and  $\omega_0/2\pi \lesssim 10^8$  Hz). The STD contribution  $w'_{111}$ , which contributes to the  $xy$  bilinear response at  $m_z \neq 0$  only, is an order of magnitude larger than the other STD contributions and dominates the  $xy$  response except at large  $d_F$  and  $\omega_0$  ( $d_F \gtrsim 10$  nm and  $\omega_0 \gtrsim 10^9$  Hz). The SSE and STD contributions can be distinguished by their dependence on the magnetization direction  $\mathbf{m}_{\text{eq}}$ : For the dominant SSE term, the charge current in the  $x$  and  $y$ -direction is proportional to  $m_y$  or  $m_x$ , respectively,

whereas for  $m_z = 0$  the STD contribution is proportional to  $m_y(1 - m_y^2)$  and  $m_x(1 - m_x^2)$ , see Eqs. (126)–(129).

The increase of the STD contributions upon decreasing  $\omega_0$  shown in Fig. 8 reflects the increased susceptibility of the magnetization in this limit. On the other hand, the local SSE and USMR contributions, which depend on thermal magnons, depend only weakly on  $\omega_0$  for small anisotropies but decrease in the limit of very strong magnetic fields [51]. This is different for the nonlocal response, because an increase in  $\omega_0$  has a strong effect on the magnon relaxation lengths and, hence, leads to a strong increase of those contributions to the bilinear response that involve the transport of incoherent magnons across the ferromagnetic layer. The  $1/d_F$ -scaling of the STD contribution at low driving frequency shown in Fig. 9 sets in for  $|k(0)|d_F \lesssim 1$ , where  $k(0) = i\sqrt{\omega_0/D_{\text{ex}}}$ . The decrease of the local USMR contribution with increasing  $d_F$  for intermediate thicknesses seen in Fig. 9 has its origin in the  $d_F$ -dependence of the longitudinal impedance  $Z_{11\parallel}(\omega)$  in the low-frequency limit, which for  $d_F \lesssim l_T$  has a parameter window in which the effective longitudinal spin impedance  $Z_{11\parallel}(\omega)$  is proportional to  $d_F$ , see Eq. (82), whereas  $Z_{11\parallel}(\omega)$  is independent of  $d_F$  for smaller as well as larger  $d_F$ . Our findings support the claim of Sterk *et al.* [51] that the local USMR effect is independent of the ferromagnet's thickness in most parameter regimes. The monotonic field dependence of the



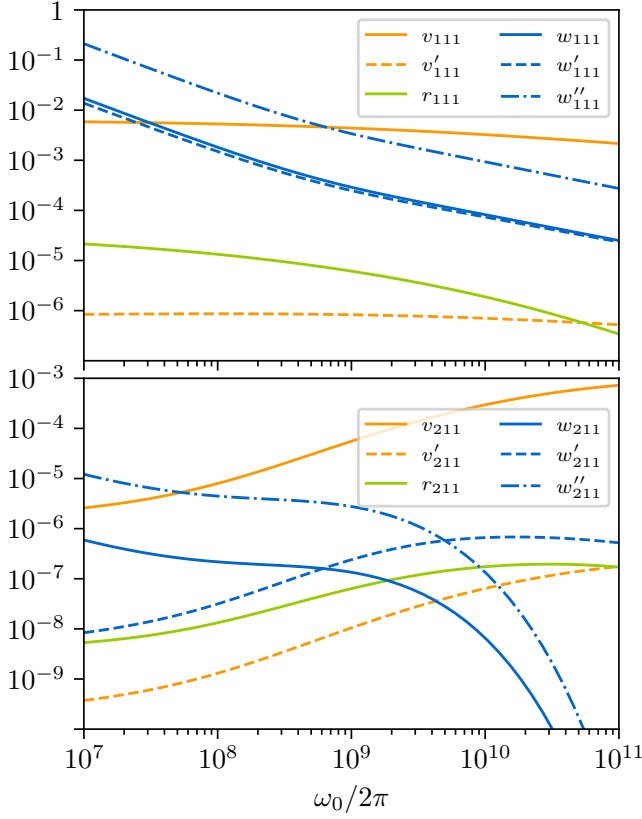


FIG. 8. Local (top) and nonlocal (bottom) dimensionless bilinear response coefficients in the limit of low driving frequency  $\omega \rightarrow 0$  as a function of the ferromagnetic resonance frequency  $\omega_0$ . Device and parameter values other than  $\omega_0$  are taken from Tabs. I and II.

USMR is specific to ferromagnetic insulators, whereas Cheng *et al.* [80] show that the antiferromagnetic USMR inherits the nonmonotonic field dependence of the antiferromagnetic magnon numbers.

In the vicinity of the resonance frequencies, the bilinear response is dominated by the STD contribution. It has sharp resonant features described by the dimensionless coefficients  $w_{i11}$ ,  $w'_{i11}$ , and  $w''_{i11}$ . For the device parameters taken here, the resonant contribution from Joule heating by dissipative spin currents, described by coefficient  $v'_{i11}$ , is smaller than the STD contributions by three orders of magnitude. For the STD contribution the coefficients of all characteristic magnetization dependences shown in Eqs. (126)–(129) have comparable magnitude.

To illustrate the scaling of the bilinear response with the device and material parameters, we now present order-of-magnitude estimates for the dimensionless bilinear response coefficients. We assume  $\omega\tau_{\text{ep}} \lesssim 1$  with electron-phonon relaxation time  $\tau_{\text{ep}}$ , so that the thermal relaxation length  $l_{\text{ep}}$  is approximately frequency-independent, as well as a large thickness  $d_F \gg l_\mu (\gg l_T)$

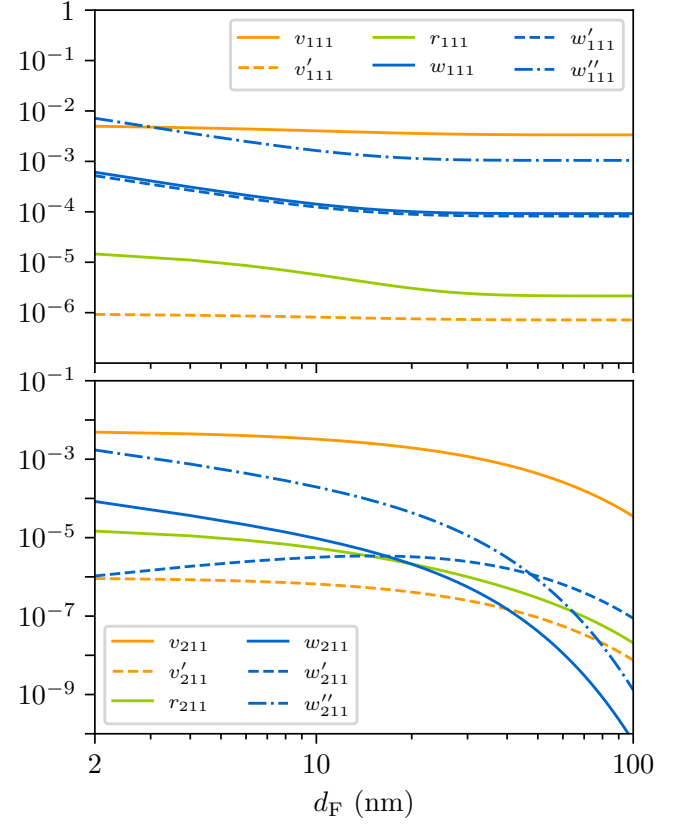


FIG. 9. Local (top) and nonlocal (bottom) dimensionless bilinear response coefficients in the limit of low driving frequency  $\omega \rightarrow 0$  as a function of the thickness  $d_F$  of the ferromagnetic layer. Device and parameter values other than  $d_F$  are taken from Tabs. I and II.

of the ferromagnetic layer. We further abbreviate

$$z_{\text{FN},i} = \frac{s}{k_{\text{T}}^3 \text{Re } g_{\uparrow\downarrow,i}}, \quad (132)$$

$$z_{\text{F}}(\Omega) = \frac{\hbar^2 D_{\text{ex}}}{2e^2 k_{\text{B}} T \sqrt{\tau_{\text{m}} \max(1/\tau_{\text{rel}}, \Omega)}}, \quad (133)$$

where  $\tau_{\text{m}}$  is the total momentum relaxation time and  $\tau_{\text{rel}} = \min(\tau_{\text{m,rel}}, \tau_{\text{mp,rel}})$  describes the faster of the two spin-non-conserving relaxation processes, and set

$$z_i(\Omega) = \max(z_{\text{FN},i}, z_{\text{F}}(\Omega)). \quad (134)$$

From the theory of Sec. IV A we obtain the order-of-

magnitude estimates

$$v_{111} \sim -\theta_{\text{SH1}} \frac{l_{\text{ep},1}}{\sigma_{\text{N1}}} \frac{1}{z_1(\Omega)}, \quad (135)$$

$$v_{211} \sim -\theta_{\text{SH2}} \frac{l_{\text{ep},1}}{\sigma_{\text{N1}}} \frac{z_{\text{F}}(\Omega)}{z_1(\Omega)z_2(\Omega)} e^{-d_{\text{F}}/l_{\mu}}, \quad (136)$$

$$v'_{111} \sim \theta_{\text{SH1}}^3 \frac{\lambda_{\text{N1}}^2 \text{Reg}_{\uparrow\downarrow 1}}{\sigma_{\text{N1}}^2} \frac{1}{z_1(\Omega)}, \quad (137)$$

$$v'_{211} \sim \theta_{\text{SH1}}^2 \theta_{\text{SH2}} \frac{\lambda_{\text{N1}}^2 \text{Reg}_{\uparrow\downarrow 1}}{\sigma_{\text{N1}}^2} \frac{z_{\text{F}}(\Omega)}{z_1 z_2} e^{-d_{\text{F}}/l_{\mu}}, \quad (138)$$

for the local and nonlocal Joule heating contributions to the bilinear response. For the local response, these expressions apply equally to the  $dc$  response at  $\Omega = 0$  and to the  $ac$  response at frequency  $\Omega = 2\omega$ . For the nonlocal response, these expressions apply for the  $dc$  and  $ac$  response at low driving frequency  $\omega$ , as well as for the  $dc$  response at large driving frequency. For the  $ac$  response at  $\Omega = 2\omega$  for large driving frequency  $\omega$ , there is a sign change with respect to the low-frequency limit and a faster decay with the thickness  $d_{\text{F}}$ ,

$$v_{211}^{\text{ac}} \sim \theta_{\text{SH2}} \frac{l_{\text{ep},1}}{\sigma_{\text{N1}}} \frac{z_{\text{F}}(\Omega)}{z_1(\Omega)z_2(\Omega)} e^{-d_{\text{F}}/l_2(\Omega)}, \quad (139)$$

$$v'_{211}{}^{\text{ac}} \sim -\theta_{\text{SH1}}^2 \theta_{\text{SH2}} \frac{\lambda_{\text{N1}}^2 \text{Reg}_{\uparrow\downarrow 1}}{\sigma_{\text{N1}}^2} \frac{z_{\text{F}}(\Omega)}{z_1 z_2} e^{-d_{\text{F}}/l_2(\Omega)}, \quad (140)$$

where  $l_2(\omega) \propto \omega^{-1/2}$  is the larger of the two relaxation lengths in F, see the discussion in Sec. III E.

In the low-frequency limit, the  $dc$  and  $ac$  contributions to the USMR and STD contributions to the bilinear response scale as

$$r_{111} \sim -\theta_{\text{SH1}}^3 \frac{i_{\text{N1}}}{i_{\text{FN1}}} \frac{\lambda_{\text{N1}}^2}{\sigma_{\text{N1}}^2} \frac{1}{z_1 z_{\text{FN},1}}, \quad (141)$$

$$r_{211} \sim -\theta_{\text{SH1}}^2 \theta_{\text{SH2}} \frac{i_{\text{N2}}}{i_{\text{FN2}}} \frac{\lambda_{\text{N1}}^2}{\sigma_{\text{N1}}^2} \frac{z_{\text{F}}^2}{z_1^2 z_2^2} e^{-2d_{\text{F}}/l_{\mu}}, \quad (142)$$

$$w_{111} \sim \theta_{\text{SH1}}^3 \frac{i_{\text{N1}}}{i_{\text{F}}} \frac{\lambda_{\text{N1}}^2}{\sigma_{\text{N1}}^2} \text{Reg}_{\uparrow\downarrow 1}^2, \quad (143)$$

$$w_{211} \sim \theta_{\text{SH1}}^2 \theta_{\text{SH2}} \frac{i_{\text{N2}}}{i_{\text{F}}} \frac{\lambda_{\text{N2}} \lambda_{\text{N1}}^2}{\sigma_{\text{N2}} \sigma_{\text{N1}}^2} \text{Im}(g_{\uparrow\downarrow 1} g_{\uparrow\downarrow 2}) \frac{z_{\text{F}}}{z_1 z_2} e^{-d_{\text{F}}/l_{\mu}}, \quad (144)$$

$$w'_{211} \sim \theta_{\text{SH1}}^2 \theta_{\text{SH2}} \frac{i_{\text{N2}}}{i_{\text{F}}} \frac{\lambda_{\text{N1}}^2}{\sigma_{\text{N1}}^2} \text{Im} g_{\uparrow\downarrow 1} \frac{z_{\text{F}}}{z_1 z_2} e^{-d_{\text{F}}/l_{\mu}}, \quad (145)$$

$$w''_{211} \sim \theta_{\text{SH1}}^2 \theta_{\text{SH2}} \frac{i_{\text{N2}}}{i_{\text{F}}} \frac{\lambda_{\text{N2}} \lambda_{\text{N1}}^2}{\sigma_{\text{N2}} \sigma_{\text{N1}}^2} \text{Re}(g_{\uparrow\downarrow 1} g_{\uparrow\downarrow 2}) \frac{z_{\text{F}}}{z_1 z_2} e^{-d_{\text{F}}/l_{\mu}}, \quad (146)$$

with the caveat that the numerical prefactor for  $r_{111}$ , which is not included in Eq. (141), is  $\sim 10^{-2}$ . The characteristic current densities  $i_{\text{N}i}$ ,  $i_{\text{FN}i}$ , and  $i_{\text{F}}$  were defined in Eqs. (92), (102), and (72), respectively. The local bilinear response coefficients  $w'_{111}$  and  $w''_{111}$  have the same order of magnitude as  $w_{111}$ .

At finite driving frequencies  $\omega$ , the local  $dc$  and  $ac$  USMR response  $r_{111}$  stays of the order of magnitude given in the zero-frequency estimate, Eq. (141), and the estimate (142) for the nonlocal USMR response  $r_{211}$  also applies to the  $dc$  response at finite driving frequency. However, the nonlocal  $ac$  response is exponentially suppressed with  $-d_{\text{F}}/l_2(\Omega)$ . As Sterk *et al.* [51], we find that for YIG and Pt, the USMR effect is negligible compared to the spin-Seebeck effect from Joule heating, which has a similar experimental signature. Only in a nonlocal measurement do we expect that there is a chance to observe the USMR signal with a characteristic magnetization dependence  $\propto m_x/m_y^2$ .

The bilinear STD response at large driving frequency  $\omega$  is dominated by resonances at  $\omega = \omega_n$  and  $\omega = \omega_n/2$ , see Eq. (76). The peak value of the nonlinear STD response at the resonances  $\omega = \omega_n$  scales as

$$|w_{111}^{\text{dc}}|_{\text{peak}} \sim |w_{111}^{\text{ac}}|_{\text{peak}} \sim \theta_{\text{SH1}}^3 i_{\text{N1}} \frac{\lambda_{\text{N1}}^2}{\sigma_{\text{N1}}^2} \frac{e}{\hbar \omega_n} \text{Reg}_{\uparrow\downarrow 1}, \quad (147)$$

with the same estimate for the peaks of the response coefficients  $w'_{111}$  and  $w''_{111}$ . Similarly, we find for the nonlocal bilinear  $dc$  STD response at the resonance peaks

$$|w_{211}^{\text{dc}}|_{\text{peak}} \sim \theta_{\text{SH1}}^2 \theta_{\text{SH2}} i_{\text{N2}} \frac{\lambda_{\text{N1}}^2}{\sigma_{\text{N1}}^2} \frac{e}{\hbar \omega_n} \text{Reg}_{\uparrow\downarrow 1}, \quad (148)$$

whereas  $w_{211}$  and  $w''_{211}$  scale with the exponent  $-d_{\text{F}}/l_2(\Omega)$  and are therefore several orders of magnitude smaller than  $w'_{211}$ . The nonlocal  $ac$  resonant STD response for all  $w_{211}$ ,  $w'_{211}$ , and  $w''_{211}$  is of a similar magnitude as  $|w'_{211}|_{\text{peak}}$ , although the individual peak heights vary with  $\cos(k(\omega)d_{\text{F}})$ , see the perpendicular impedances in Eqs. (57) and (58).

## V. DISCUSSION AND CONCLUSION

The comprehensive theory discussed in this article describes magnon-mediated transport effects in multilayers combining ferromagnetic insulators and normal metals for driving frequencies ranging from the  $dc$  limit well into the  $ac$  (THz) regime. Our approach, which describes the coupling across the magnetic-insulator-normal-metal interface using the spin-mixing conductance and otherwise relies on semi-phenomenological transport equations, establishes a consistent, unified description of a plethora of spintronic effects reported in the literature. These include the spin-Hall magnetoresistance [15–17, 52], nonlocal spin-Hall magnetoresistance or magnon-mediated electric current drag [18, 24, 25], nonlocal magnon-mediated magnetoresistance [50], the spin-Seebeck effect [40] and its inverse — the spin-Peltier effect [62] —, Joule heating from spin currents [75, 76], spin-orbit torque [39, 40], unidirectional magnetoresistance (UMR) [39], and magnonic unidirectional spin-Hall magnetoresistance (USMR) [38, 40, 51]. Having a common theoretical framework allows a quantitative comparison between

the discussed mechanisms and between different driving frequencies.

Depending on driving frequency, the same or similar phenomena can take place via different physical mechanisms. As discussed in detail in Sec. III E, for low frequencies the nonlocal linear electrical conductivity is mediated by incoherent magnons, driven by a gradient of the magnon chemical potential in the ferromagnetic insulator F [34]. When approaching the GHz regime, the magnon chemical potential can no longer adapt to the fast variations of the driving field and the nonlocal charge current is suppressed. This suppression, however, does not apply for the resonant coherent spin waves, which dominate the nonlocal response for driving frequencies in the GHz regime and above.

The picture is more complex in the bilinear response, where multiple mechanisms have been discussed in the literature. Via the linear coupling between spin and heat currents at the interface between the magnetic insulator and the normal metal N, Joule heating in N drives a spin current through the interface, which, via the inverse spin-Hall effect, gives rise to a charge current in N. Many experiments observe such Joule heating effects as a second harmonic response to an *ac* field [81, 82]. Our theory confirms that for small or off-resonant frequencies, this assumption often holds. There are, however, certain parameter regimes where Joule heating is not the dominant contribution. This includes small magnetic anisotropies, small thicknesses of F and a driving frequency close to resonant frequencies of coherent magnons. In these instances, the spin-torque diode (STD) effect can predominate [5, 40]. A subordinate role is played by the interfacial magnonic USMR, which we find to be at least two orders of magnitude smaller than Joule heating or STD in the *dc* limit. The USMR effect is significantly larger in magnetic metals [38], where the largest contribution is from the electronic spin accumulation not present in insulators. In addition, the latter have a smaller thermal conductivity, which results in inhomogeneous heating in F and N and ultimately to Joule heating as the dominant second-order-in-*E* response [51].

Since all three bilinear contributions change sign under reversal of the magnetization direction, they constitute a unidirectional magnetoresistance (UMR) in F|N multilayers. Unidirectional effects are also present in heterostructures with antiferromagnetic-insulator [80, 83–85], topological-insulator [86], or magnetic-metal [38, 39] layers and their origins differ between those systems. Recent years have shown a particular interest in antiferromagnetic UMR, which is driven by both magnon dynamics — altered by a field-induced spin canting — and an interfacial Rashba splitting [83, 84]. We note that antiferromagnetic UMR effects show a different experimental signature compared to the ferromagnetic effects discussed here; especially with regard to its dependence on external magnetic fields.

We also point out some limitations to our theory. Experiments suggest that magnon transport in YIG persists

on longer length scales than predicted by the relaxation time approximation made in our semi-phenomenological transport theory [21]. We attribute this difference to a strong frequency dependence of the relaxation times, which is not captured by our description. As a result, subthermal, but still incoherent magnons (magnon frequency  $\sim 10$  GHz, see Ref. 64), carry most of the spin at room temperature [74]. A microscopic description of the scattering processes, accompanied by a spectrally resolved description of the spin conductance (as in, *e.g.*, Ref. 35, and in contrast to a cumulative description [64]) would likely improve quantitative predictions. Furthermore, our semi-phenomenological transport theory neglects the wave-like nature of electrons in N and, hence, disregards any quantum interference effects that may contribute to UMR [87].

From a practical point of view, N|F|N trilayers offer a toolbox with several spintronic applications. In addition to the magnetic state of F, we have demonstrated that also the driving frequency determines the direction and magnitude of the nonlocal drag current. A spin valve design and control of the local resistance is possible already at zero frequency in linear response. Bilinear unidirectional effects allow for the detection of magnetization switching in a two-terminal setup [38].

A consequence of the linear coupling of spin and heat currents across the F|N interfaces is that heat currents can be driven into or out of the normal metal to linear order in the applied electric field. The sign of these heat currents depends on the sign of the electric field, so that not only current-induced heating, but also current-induced cooling of electrons in N is possible (at the expense of heating up the magnons in F) [62]. The maximum temperature difference that can be obtained in such a spin-Peltier effect is bounded by competition with effects quadratic in the applied electric field, first and foremost the Joule heating from charge currents in N. To estimate the maximum amount of cooling that can therefore be obtained, we consider the total change of the electron temperature at the F|N interface

$$\Delta u_{eQi} = \Delta u_{eQi}^{(1)} + \Delta u_{eQi}^{(2)}, \quad (149)$$

where the bilinear part (evaluated at zero frequency) is

$$\begin{aligned} \Delta u_{eQi}^{(2)} &= \delta u_{eQi} + (-1)^{i-1} Z_{QNi} i_{Qi} \\ &= \delta u_{eQi} - \sum_j (-1)^{i+j} Z_{QNj} \left[ Z_{ij}^{-1} \right]_{QT} \delta u_{eQj}. \end{aligned} \quad (150)$$

Comparing local and nonlocal cooling effects (*i.e.*, in the same layer as where the electric field is applied or in the opposite layer), we find that, because of the strongly suppressed Joule heating in the opposite N layer, the nonlocal cooling effect is strongest, with a maximum  $\Delta T_e = (e/k_B) \Delta u_{eQe} \approx -0.6$  mK at  $E \approx 2$  V  $\mu\text{m}^{-1}$  for the device parameters used in this article. Local cooling is considerably weaker and we find at most  $\Delta T_e \approx -0.02$  mK at applied field  $E \approx 0.005$  V  $\mu\text{m}^{-1}$ . For these estimates, we recall that our semi-phenomenological transport equations

for N as well as F include heat exchange with the phonon bath, assuming a phonon heat capacity large enough that the phonon bath temperature stays constant, see Sec. III. We do not consider the effect of the temperature modulation on the resistivity of Pt — an effect that Sullivan *et al.* [88] associate with a phonon-mediated magnetoresistance.

The spin-Peltier effect has been observed by Flipse *et al.* [62] for Pt|YIG bilayers. Thermal imaging by Daimon *et al.* [89] underscores that the spin-Peltier effect allows pinpoint modulation of the temperature in the mK regime, as predicted by our theory. Chiriaco and Millis [90] found a related effect in electronic systems with interfaces between metallic and insulating phases, in particular  $\text{Ca}_2\text{RuO}_4$ , where the spatial discontinuity of the Seebeck coefficient drives Peltier cooling, which competes with Joule heating. The nonlocal spin-Peltier effect has not been observed experimentally. In view of the large upper bound for the nonlocal effect (see the discussion above), we believe that an experimental search for this effect is promising.

## ACKNOWLEDGMENTS

We thank T. Kampfrath for stimulating discussions. This work was funded by the Deutsche Forschungsgemeinschaft (DFG, German Research Foundation) through the Collaborative Research Center SFB TRR 227 “Ultrafast spin dynamic” (Project-ID 328545488, project B03).

## Appendix A: Derivation of phenomenological transport equations from Boltzmann theory

In this Appendix, we derive expressions for the matrices  $\mathcal{C}_m$  in Eq. (43),  $\mathcal{G}_m$  in Eq. (45), and  $\Sigma(\omega)$  in Eq. (47), whose numerical estimates are presented in Tab. II.

We express the magnon spin and energy density in terms of the magnon distribution function  $n_{\mathbf{k}}(z, t)$ , which we linearize around the equilibrium distribution function  $n^0(\omega_{\mathbf{k}}) = 1/(e^{\hbar\omega_{\mathbf{k}}/k_B T} - 1)$ ,

$$n_{\mathbf{k}}(z, t) = n^0(\omega_{\mathbf{k}}) + \left(-\frac{\partial n^0}{\partial \omega_{\mathbf{k}}}\right) \psi_{\mathbf{k}}(z, t). \quad (\text{A1})$$

Consistent with a description in terms of magnon spin and energy density and the corresponding currents, for the deviation from equilibrium  $\psi_{\mathbf{k}}(z, t)$  we use the *Ansatz*

$$\begin{aligned} \psi_{\mathbf{k}}(z, t) = & \frac{1}{\hbar} \mu_m(z, t) + \frac{\omega_{\mathbf{k}}}{T} \Delta T_m(z, t) \\ & + v_{\mathbf{k}z} \left[ \frac{1}{\hbar} \pi_{m\mu}(z, t) + \frac{\omega_{\mathbf{k}}}{T} \pi_{mT}(z, t) \right], \end{aligned} \quad (\text{A2})$$

where  $\mu_m = e u_m$  is the local magnon chemical potential,  $\Delta T_m = (e/k_B) \Delta u_{mQ}$  the difference between the local magnon temperature and the temperature  $T$  of the

phonon bath (which we assume to be constant), and  $\pi_{m\mu}$  and  $\pi_{mT}$  are generalized potentials that determine the magnon spin and energy currents.

In terms of the distribution function  $n_{\mathbf{k}}(z, t)$ , the excess magnon spin density  $\rho_{ms}(z, t)$  reads (using equivalent charge units)

$$\rho_{ms}(z, t) = \frac{2e}{(2\pi)^3} \int d\mathbf{k} \left(-\frac{\partial n^0}{\partial \omega_{\mathbf{k}}}\right) \psi_{\mathbf{k}}(z, t). \quad (\text{A3})$$

Substitution of the *Ansatz* (A2) then gives

$$\rho_{ms}(z, t) = c_{m,s\mu} u_m(z, t) + c_{m,sT} \Delta u_{mQ}(z, t), \quad (\text{A4})$$

with

$$\begin{aligned} c_{m,s\mu} &= (2e^2/\hbar) F_{0,0}, \\ c_{m,sT} &= (2e^2/\hbar) F_{0,1}. \end{aligned} \quad (\text{A5})$$

Here we introduced the moments

$$\begin{aligned} F_{m,n} &= \frac{1}{(2\pi)^3} \\ &\times \int d\mathbf{k} \left( \frac{\hbar v_{\mathbf{k}z}^2}{4D_{\text{ex}} k_B T} \right)^m \left( \frac{\hbar \omega_{\mathbf{k}}}{k_B T} \right)^n \left( -\frac{\partial n^0}{\partial \omega_{\mathbf{k}}} \right). \end{aligned} \quad (\text{A6})$$

Similarly, the excess magnon energy density  $\rho_{mQ}(z, t)$  is

$$\rho_{mQ}(z, t) = \frac{2e}{(2\pi)^3 k_B T} \int d\mathbf{k} \hbar \omega_{\mathbf{k}} \left( -\frac{\partial n^0}{\partial \omega_{\mathbf{k}}} \right) \psi_{\mathbf{k}}(z, t), \quad (\text{A7})$$

which we write as

$$\rho_{mQ}(z, t) = c_{m,Q\mu} u_m(z, t) + c_{m,QT} \Delta u_{mQ}(z, t), \quad (\text{A8})$$

with

$$\begin{aligned} c_{m,Q\mu} &= (2e^2/\hbar) F_{0,1} \\ c_{m,QT} &= (2e^2/\hbar) F_{0,2}. \end{aligned} \quad (\text{A9})$$

Equations (A3)–(A9) reproduce the matrix relation (43) and provide microscopic expressions for the coefficients of the matrix  $\mathcal{C}_m$ . For the magnon spin current density  $i_{s\parallel}(z, t)$  and the magnon heat current density  $i_Q(z, t)$  we find in the same manner

$$\begin{pmatrix} i_{s\parallel}(z, t) \\ i_Q(z, t) \end{pmatrix} = \mathcal{V}_m \begin{pmatrix} \pi_{m\mu}(z, t)/e \\ k_B \pi_{mT}(z, t)/e \end{pmatrix}, \quad (\text{A10})$$

where

$$\begin{aligned} \mathcal{V}_m &= \frac{2e^2}{\hbar} \int \frac{d\mathbf{k}}{(2\pi)^3} v_{\mathbf{k}z}^2 \left( -\frac{\partial n^0}{\partial \omega_{\mathbf{k}}} \right) \\ &\times \begin{pmatrix} 1 & \hbar \omega_{\mathbf{k}}/k_B T \\ \hbar \omega_{\mathbf{k}}/k_B T & (\hbar \omega_{\mathbf{k}}/k_B T)^2 \end{pmatrix} \\ &= \frac{2e^2}{\hbar} \frac{4D_{\text{ex}} k_B T}{\hbar} \begin{pmatrix} F_{1,0} & F_{1,1} \\ F_{1,1} & F_{1,2} \end{pmatrix}. \end{aligned} \quad (\text{A11})$$

Explicit expressions for the moments  $F_{mn}$  may be obtained for the magnon dispersion

$$\omega_k = \omega_0 + D_{\text{ex}} k^2. \quad (\text{A12})$$

In this case, the integrations over  $\mathbf{k}$  in Eq. (A6) can be replaced by integrations over  $\omega$  and one finds

$$\begin{aligned} F_{m,n} &= \frac{1}{2m+1} \frac{1}{4\pi^2 D_{\text{ex}}^{3/2}} \int d\omega \sqrt{\omega - \omega_0} \\ &\quad \times \left( \frac{\hbar(\omega - \omega_0)}{k_B T} \right)^m \left( \frac{\hbar\omega}{k_B T} \right)^n \left( -\frac{\partial n^0}{\partial \omega} \right) \\ &= \frac{1}{2m+1} \sqrt{\frac{k_B T}{\hbar D_{\text{ex}}^3}} \int_{\xi_0}^{\infty} d\xi \frac{\xi^n (\xi - \xi_0)^{m+1/2}}{16\pi^2 \sinh^2(\xi/2)}, \end{aligned} \quad (\text{A13})$$

where  $\xi_0 = \hbar\omega_0/k_B T$ . For  $n = 0$ , one thus finds

$$F_{m,0} = \frac{\Gamma(m+1/2)}{8\pi^2 D_{\text{ex}}} \sqrt{\frac{k_B T}{\hbar D_{\text{ex}}}} \text{Li}_{m+1/2}(e^{-\xi_0}), \quad (\text{A14})$$

where  $\text{Li}(z)$  is the polylogarithm and  $\Gamma$  the gamma function, whereas moments  $F_{m,n}$  with  $n = 1$  and  $n = 2$  can be obtained from the recursion relations

$$\begin{aligned} F_{m,1} &= \xi_0 F_{m,0} + \frac{2m+3}{2m+1} F_{m+1,0}, \\ F_{m,2} &= \xi_0^2 F_{m,0} + 2 \frac{2m+3}{2m+1} \xi_0 F_{m+1,0} \\ &\quad + \frac{2m+5}{2m+1} F_{m+2,0}. \end{aligned} \quad (\text{A15})$$

Numerical values for the coefficients of  $\mathcal{C}_m$ , using the parameters listed in Tab. I, are given in Tab. II. In the limit  $\xi_0 \ll 0$ , which is applicable to YIG at room temperature, one may approximate

$$\begin{aligned} F_{m,n} &\approx \frac{\Gamma(m+n+1/2)}{8\pi^2 D_{\text{ex}}} \sqrt{\frac{k_B T}{\hbar D_{\text{ex}}}} \\ &\quad \times \begin{cases} \sqrt{\pi/\xi_0} & \text{if } m = n = 0, \\ \frac{2m+2n+1}{2m+1} \zeta(m+n+1/2) & \text{if } m+n > 0, \end{cases} \end{aligned} \quad (\text{A16})$$

with Riemann zeta function  $\zeta$ .

Our estimate for the volumetric magnon heat capacity  $c_{m,\text{QT}}$  is (numerically) close to the result obtained in Ref. 74 and agrees with experimental data at low temperatures  $T < 10$  K. At room temperature it is difficult to directly measure the magnon contribution to the heat capacity by taking the difference of high-magnetic-field and low-field heat capacities because of the large magnetic field needed to freeze out magnons [91]. Experiment [74] and theory [91] show that the increase of heat capacity at higher temperatures is likely to be slower than  $T^{3/2}$ . Although this means that Eq. (A9) probably overestimates the magnon heat capacity at  $T = 300$  K, the numerical value obtained from Eq. (A9) is still of the same order of magnitude as other values given in the literature, see, e.g., Ref. 91.

To find expressions for the matrices  $\mathcal{G}_m$  and  $\Sigma_m$ , introduced in the spin continuity Eq. (16) and Ohm's law for thermal magnons in Eq. (46), respectively, we use the Boltzmann equation for the linearized distribution function  $\psi_{\mathbf{k}}(z, t)$ ,

$$\frac{\partial \psi_{\mathbf{k}}(z, t)}{\partial t} + v_{\mathbf{k},z} \frac{\partial \psi_{\mathbf{k}}(z, t)}{\partial z} = \sum_{\alpha} \int d\mathbf{k}' \Gamma_{\mathbf{k},\mathbf{k}'}^{(\alpha)} \psi_{\mathbf{k}'}(z, t) \quad (\text{A17})$$

where the summation is over different relaxation processes, labeled by  $\alpha$ , and  $\Gamma_{\mathbf{k},\mathbf{k}'}^{(\alpha)}$  denotes the corresponding transition rates. To obtain closed equations for  $\mu_m(z, t)$  and  $\Delta T_m(z, t)$ , we multiply Eq. (A17) by  $\hbar(-\partial n^0/\partial \omega_{\mathbf{k}})$  and by  $\hbar\omega_{\mathbf{k}}(-\partial n^0/\partial \omega_{\mathbf{k}})$ , substitute the Ansatz (A2) for the linearized distribution function, and integrate over  $\mathbf{k}$ . Integrals on the r.h.s. containing odd powers of  $v_{\mathbf{k}z}$  vanish, so that the r.h.s. is a linear function of  $\mu_m(z, t)$  and  $\Delta T_m(z, t)$  only. The resulting equation has the form of Eq. (44), with

$$\begin{aligned} \mathcal{G}_m &= -\frac{\hbar}{2e^2} \int \frac{d\mathbf{k} d\mathbf{k}'}{(2\pi)^3} \left( -\frac{\partial n^0}{\partial \omega_{\mathbf{k}}} \right) \\ &\quad \times \sum_{\alpha} \Gamma_{\mathbf{k},\mathbf{k}'}^{(\alpha)} \left( \frac{1}{\hbar\omega_{\mathbf{k}}/k_B T} \frac{\hbar\omega_{\mathbf{k}}/k_B T}{(\hbar\omega_{\mathbf{k}}/k_B T)^2} \right). \end{aligned} \quad (\text{A18})$$

The relaxation-time approximation corresponds to the simple choice

$$\Gamma_{\mathbf{k},\mathbf{k}'}^{(\alpha)} = -\frac{1}{\tau_{\alpha}} \left[ \delta_{\mathbf{k},\mathbf{k}'} - \frac{1}{(2\pi)^3} \left( -\frac{\partial n^0}{\partial \omega_{\mathbf{k}}} \right) c_{\mathbf{k},\mathbf{k}'}^{(\alpha)} \right], \quad (\text{A19})$$

where  $\delta_{\mathbf{k},\mathbf{k}'}$  is the Dirac delta function and  $\tau_{\alpha}$  is the relaxation time, which is independent of  $\mathbf{k}$ . The second term between the square brackets is a phenomenological correction term that ensures conservation of magnon spin density and/or magnon energy density, if applicable. We consider five relaxation processes for magnons: exchange-based spin-conserving magnon-magnon ( $\alpha = \text{"m, ex"}$ ) and magnon-phonon scattering ( $\alpha = \text{"mp, ex"}$ ), relativistic spin-non-conserving magnon-magnon ( $\alpha = \text{"m, rel"}$ ) and magnon-phonon scattering ( $\alpha = \text{"mp, rel"}$ ), and elastic magnon-impurity scattering ( $\alpha = \text{"el"}$ ). For elastic magnon-impurity scattering, which relaxes the magnon currents, but not the magnon spin and energy densities, and for exchange-based magnon-magnon scattering one has

$$c_{\mathbf{k},\mathbf{k}'}^{(\alpha)} = \frac{2e^2}{\hbar} (1 - \hbar\omega_{\mathbf{k}}/k_B T) \mathcal{C}_m^{-1} \left( \frac{1}{\hbar\omega_{\mathbf{k}}/k_B T} \right), \quad (\text{A20})$$

with  $\alpha = \text{"m, ex"}$  or  $\alpha = \text{"el"}$ . (If umklapp processes were ruled out, exchange-based magnon-magnon scattering would also conserve magnon momentum density, which would result in a modified correction term.) Similarly, for exchange-based magnon-phonon scattering, which conserves magnon spin density, but not magnon



energy density, and for relativistic three-magnon scattering, which conserves magnon energy density, but not the magnon spin density, one has

$$c_{\mathbf{k},\mathbf{k}'}^{\text{mp,ex}} = \frac{2e^2}{\hbar} \frac{1}{c_{\text{m},s\mu}}, \quad (\text{A21})$$

$$c_{\mathbf{k},\mathbf{k}'}^{\text{m,rel}} = \frac{2e^2}{\hbar} \left( \frac{\hbar}{k_B T} \right)^2 \frac{\omega_{\mathbf{k}} \omega_{\mathbf{k}'}}{c_{\text{m},\text{QT}}}. \quad (\text{A22})$$

Finally, for relativistic magnon-phonon scattering, which conserves neither the magnon spin density nor the magnon current density, one may set

$$c_{\mathbf{k},\mathbf{k}'}^{\text{mp,rel}} = 0. \quad (\text{A23})$$

Calculating the four elements of the relaxation matrix  $\mathcal{G}_{\text{m}}$  in the relaxation-time approximation (A19) then results in Eq. (50) of the main text.

Numerical estimates for the scattering times are given in Tab. II. Without the terms proportional to  $\gamma$  and upon identifying (notation of Ref. 34)  $\Gamma_{s\mu} = \tau_{\text{mp,rel}}^{-1} + \tau_{\text{m,rel}}^{-1}$  and  $\Gamma_{\text{QT}} = \tau_{\text{mp,rel}}^{-1} + \tau_{\text{mp,ex}}^{-1}$  as well as the cross terms  $\Gamma_{\text{ST}} = \tau_{\text{mp,rel}}^{-1} c_{\text{m},\text{QT}}^{-1} c_{\text{m},\text{ST}}$  (in  $1/\text{Js}$ ) and  $\Gamma_{Q\mu} = -\tau_{\text{mp,rel}}^{-1} c_{\text{m},\text{ST}} c_{\text{m},s\mu}^{-1}$ , Eqs. (44) and (50) reproduce the spin and heat continuity equations for magnon transport from Ref. 34.

In a similar manner, the linear-response equation (46) can be obtained from the Boltzmann equation (A17) upon multiplication by  $(2e/\hbar)\hbar v_{\mathbf{k}z}(-\partial n^0/\partial \omega_{\mathbf{k}})$  and by  $(2e/k_B T)\hbar \omega_{\mathbf{k}} v_{\mathbf{k}z}(-\partial n^0/\partial \omega_{\mathbf{k}})$ , followed by integration over  $\mathbf{k}$ . This gives

$$\frac{\partial}{\partial t} \begin{pmatrix} i_{s\parallel} \\ i_Q \end{pmatrix} + \mathcal{V}_{\text{m}} \frac{\partial}{\partial z} \begin{pmatrix} u_{\text{m}} \\ \Delta u_{\text{mQ}} \end{pmatrix} = -\tau_{\text{m}}^{-1} \begin{pmatrix} i_{s\parallel} \\ i_Q \end{pmatrix} \quad (\text{A24})$$

where  $\tau_{\text{m}}$  is a  $2 \times 2$  matrix defined as

$$\tau_{\text{m}}^{-1} = \sum_{\alpha} \tau_{\text{m}}^{(\alpha)-1}, \quad (\text{A25})$$

with

$$\tau_{\text{m}}^{(\alpha)-1} \mathcal{V}_{\text{m}} = -\frac{2e^2}{\hbar} \int \frac{d\mathbf{k} d\mathbf{k}'}{(2\pi)^3} \left( -\frac{\partial n^0}{\partial \omega_{\mathbf{k}}} \right) \Gamma_{\mathbf{k},\mathbf{k}'}^{(\alpha)} v_{\mathbf{k}z} v_{\mathbf{k}'z} \\ \times \begin{pmatrix} 1 & \hbar \omega_{\mathbf{k}}/k_B T \\ \hbar \omega_{\mathbf{k}}/k_B T & (\hbar \omega_{\mathbf{k}}/k_B T)^2 \end{pmatrix}. \quad (\text{A26})$$

Hence, Eq. (46) follows, with

$$\Sigma(\omega) = (\mathbb{1} - i\omega \tau_{\text{m}})^{-1} \tau_{\text{m}} \mathcal{V}_{\text{m}}, \quad (\text{A27})$$

where  $\mathbb{1}$  is the  $2 \times 2$  unit matrix. In the relaxation-time approximation (A19) one has

$$\tau_{\text{m}}^{-1} = \mathbb{1} \sum_{\alpha} \tau_{\alpha}^{-1}, \quad (\text{A28})$$

consistent with Eq. (52). For the magnon conductivity  $\sigma_{\text{m}}$ , the spin-Seebeck coefficient  $L_{\text{m}}$ , and the magnon

thermal conductivity  $\kappa_{\text{m}}$ , we thus find, in the relaxation-time approximation

$$\sigma_{\text{m}} = \frac{8e^2 \tau_{\text{m}} D_{\text{ex}} k_B T}{\hbar^2} F_{1,0}, \quad (\text{A29})$$

$$L_{\text{m}} = \frac{8e \tau_{\text{m}} D_{\text{ex}} k_B^2 T^2}{\hbar^2} F_{1,1}, \quad (\text{A30})$$

$$\kappa_{\text{m}} = \frac{4\tau_{\text{m}} D_{\text{ex}} k_B^3 T^2}{\hbar^2} F_{1,2}. \quad (\text{A31})$$

These three results agree with Ref. 34. We may overestimate  $\kappa_{\text{m}}$  at room temperature since the total thermal conductivity of YIG is only two times larger than our prediction for  $\kappa_{\text{m}}$  [92] and the magnon contribution is consequently often assumed to be smaller, *e.g.*, in Ref. 93. Since we adjusted magnon impurity scattering to correctly reproduce the spin conductivity, we obtain a similar  $\sigma_{\text{m}}$  as measured in Ref. 21.

## Appendix B: Bilinear response

In this appendix, we present additional details for the calculation of the nonlinear response in Sec. IV.

### Bilinear SSE response and Joule heating

The Joule heating rate is [75, 76]

$$s(\mathbf{r}, t) = -\frac{1}{e} \nabla \cdot (\mathbf{i}(\mathbf{r}, t) \cdot \varphi_c(\mathbf{r}, t)) \\ - \frac{1}{\hbar} \nabla \cdot (\mathbf{j}_s(\mathbf{r}, t) \cdot \boldsymbol{\mu}_s(\mathbf{r}, t)), \quad (\text{B1})$$

where  $\varphi_c(\mathbf{r}, t)$  is the electrochemical potential,  $\mathbf{j}_s(\mathbf{r}, t) = (\hbar/2e)\mathbf{i}_s(\mathbf{r}, t)$  the spin current tensor, and  $\boldsymbol{\mu}_s(\mathbf{r}, t) = e\mathbf{u}_s(\mathbf{r}, t)$  the spin accumulation. The charge current density  $i^z(\mathbf{r}, t) = 0$ , whereas  $i^x(\mathbf{r}, t)$  and  $i^y(\mathbf{r}, t)$  depend on  $z$  only. The electrochemical potential  $\varphi_c(\mathbf{r}, t)$  does not depend on  $y$ . Hence, the first term in Eq. (B1) simplifies to  $-(1/e)(i^x(z, t)\partial \varphi_c(\mathbf{r}, t)/\partial x = i^x(z, t)E_x(t))$ . For the second term, we note that both  $\mathbf{i}_s(\mathbf{r}, t)$  and  $\mathbf{u}_s(\mathbf{r}, t)$  depend on  $z$  only, so that Eq. (88) of the main text follows.

Using Eqs. (11)–(18), the charge and spin current densities N1 can be expressed in terms of the applied field  $E_1(t)$  and the spin accumulation  $\mathbf{u}_{s1}(t)$  at the F|N1 interface at  $z = 0$ ,

$$\mathbf{u}_s(z, t) = \mathbf{u}_{s1}(t) e^{-z/\lambda_{N1}}, \quad (\text{B2})$$

$$i^x(z, t) = \sigma_{N1} E_1(t) + \frac{\theta_{\text{SH1}} \sigma_{N1}}{2\lambda_{N1}} e^{-z/\lambda_{N1}} \mathbf{u}_{s1}(t) \cdot \mathbf{e}_y,$$

$$i_s^z(z, t) = -\theta_{\text{SH1}} \sigma_{N1} E_1(t) \mathbf{e}_y + \frac{\sigma_{N1}}{2\lambda_{N1}} e^{-z/\lambda_{N1}} \mathbf{u}_{s1}(t),$$

with analogous equations for the charge and spin current densities in N2. From Eq. (88) we then find the local

Joule heating rates

$$s_1(z, t) = \sigma_{N1} E_1(t)^2 + \frac{\sigma_{N1}}{2\lambda_{N1}^2} |\mathbf{u}_{s1}(t)|^2 e^{-2z/\lambda_{N1}}, \quad (\text{B3})$$

$$s_2(z, t) = \sigma_{N2} E_2(t)^2 + \frac{\sigma_{N2}}{2\lambda_{N2}^2} |\mathbf{u}_{s2}(t)|^2 e^{-2(d_F - z)/\lambda_{N2}}.$$

in N1 and N2, respectively.

Inserting Eq. (B3) into Eq. (91) and performing a Fourier transform, the source terms  $\delta u_{eQi}(\Omega)$  in the

boundary condition (90) become

$$\delta u_{eQi}(\Omega) = \frac{k_B^2 l_{ep,i}(\Omega)^2 \sigma_{Ni}}{2\pi e^2 \kappa_{ei}} \int d\omega \left[ E_i(\omega_+) E_i(-\omega_-) + \frac{\mathbf{u}_{si}(\omega_+) \cdot \mathbf{u}_{si}(-\omega_-)}{4\lambda_{Ni} l_{ep,i}(\Omega)} f_i(\omega) \right], \quad (\text{B4})$$

where we abbreviated (assuming  $d_{Ni} \gg \lambda_{Ni}$ )

$$f_i(\Omega) = \frac{4l_{ep,i}(\Omega)^2 \coth(d_{Ni}/l_{ep,i}(\Omega)) - 2l_{ep,i}(\Omega)\lambda_{Ni}}{4l_{ep,i}(\Omega)^2 - \lambda_{Ni}^2}. \quad (\text{B5})$$

The interfacial spin accumulations  $\mathbf{u}_{si}(\pm\omega_{\pm})$  can be expressed in terms of the electric field, see Eq. (63). For the source term  $\delta u_{eQi}(\Omega)$  of Eq. (B4), this gives

$$\begin{aligned} \delta u_{eQi}(\Omega) = & \frac{Z_{Ni}}{2\pi i_{Ni}} \sum_{j,k} \int d\omega E_j(\omega_+) E_k(\omega_-)^* \sigma_{Nj} \sigma_{Nk} \frac{l_{ep,i}(\Omega)}{l_{ep,i}(0)} \left\{ \frac{l_{ep,i}(\Omega)}{\lambda_{Ni}} \delta_{ij} \delta_{ik} + (-1)^{j+k} \theta_{SHj} \theta_{SHk} f_i(\Omega) \right. \\ & \times [|\mathbf{m}_{eq} \cdot \mathbf{e}_y|^2 (\delta_{ij} - \zeta_{ij\parallel}(\omega_+)) (\delta_{ik} - \zeta_{ik\parallel}(\omega_-)^*) \\ & \left. + |\mathbf{e}_{\perp} \cdot \mathbf{e}_y|^2 [(\delta_{ij} - \zeta_{ij\perp}(\omega_+)) (\delta_{ik} - \zeta_{ik\perp}(\omega_-)^*) + (\delta_{ij} - \zeta_{ij\perp}(-\omega_+)^*) (\delta_{ik} - \zeta_{ik\perp}(-\omega_-))] \right\}, \end{aligned} \quad (\text{B6})$$

where  $i_{Ni}$  is defined in Eq. (92). The first term in Eq. (B6) is the same as in Eq. (93) of the main text.

Combining Eqs. (B6), (94), and (95), we find that the charge current associated with Joule heating reads

$$i_i^x(\Omega)_{\text{Joule}}^{(2)} = \sum_{j,k=1}^2 \int \frac{d\omega}{2\pi} \frac{\lambda_{Ni}}{d_{Ni} i_{Ni}} \sigma_{Nj} \sigma_{Nk} E_j(\omega_+) E_k(\omega_-)^* [v_{ijk}(\omega_+, \omega_-) m_y + v'_{ijk}(\omega_+, \omega_-) m_y (1 - m_y^2)], \quad (\text{B7})$$

$$i_i^y(\Omega)_{\text{Joule}}^{(2)} = - \sum_{j,k=1}^2 \int \frac{d\omega}{2\pi} \frac{\lambda_{Ni}}{d_{Ni} i_{Ni}} \sigma_{Nj} \sigma_{Nk} E_j(\omega_+) E_k(\omega_-)^* [v_{ijk}(\omega_+, \omega_-) m_x + v'_{ijk}(\omega_+, \omega_-) m_x (1 - m_y^2)], \quad (\text{B8})$$

where the dimensionless coefficients  $v_{ijk}$  and  $v'_{ijk}$  read

$$\begin{aligned} v_{ijk}(\omega_+, \omega_-) = & -\theta_{SHi} \sum_{l=1}^2 \chi_{il}(\Omega) (-1)^{l-1} \frac{l_{ep,l}(\Omega)}{l_{ep,l}(0)} \\ & \times \left\{ \frac{l_{ep,l}(\Omega)}{\lambda_{Ni}} \delta_{lj} \delta_{lk} + (-1)^{j+k} \theta_{SHj} \theta_{SHk} f_l(\Omega) (\delta_{lj} - \zeta_{lj\parallel}(\omega_+)) (\delta_{lk} - \zeta_{lk\parallel}(\omega_-)^*) \right\}, \end{aligned} \quad (\text{B9})$$

$$\begin{aligned} v'_{ijk}(\omega_+, \omega_-) = & \frac{1}{2} \theta_{SHi} \theta_{SHj} \theta_{SHk} \frac{l_{ep,l}(\Omega)}{l_{ep,l}(0)} \sum_{l=1}^2 \chi_{il}(\Omega) (-1)^{l+j+k-1} f_l(\Omega) \left\{ 2(\delta_{lj} - \zeta_{lj\parallel}(\omega_+)) (\delta_{lk} - \zeta_{lk\parallel}(\omega_-)^*) \right. \\ & \left. - (\delta_{lj} - \zeta_{lj\perp}(\omega_+)) (\delta_{lk} - \zeta_{lk\perp}(\omega_-)^*) - (\delta_{lj} - \zeta_{lj\perp}(-\omega_+)^*) (\delta_{lk} - \zeta_{lk\perp}(-\omega_-)) \right\}, \end{aligned} \quad (\text{B10})$$

where  $\chi_{ji}(\omega)$  is given in Eq. (99). The first term in Eq. (B9) corresponds to Eq. (98) of the main text.

### Nonlinear longitudinal interfacial spin conductance and bilinear USMR response

The longitudinal spin current and the heat currents through the F|N interface are [34, 77]

$$\begin{aligned} i_{si\parallel}^z = & \frac{\text{Re } g_{\uparrow\downarrow i}}{\pi^2 s} \left( \frac{e}{\hbar D_{\text{ex}}} \right)^{3/2} (-1)^{i-1} \int_{u_0}^{\infty} du \sqrt{u - u_0} \\ & \times \left[ \frac{u - u_{si\parallel}}{e^{(u - u_{mi})/u_{mQi}} - 1} - \frac{u - u_{si\parallel}}{e^{(u - u_{si\parallel})/u_{eQi}} - 1} \right]. \end{aligned} \quad (\text{B11})$$

where  $u_0 = \hbar\omega_0/e$ . Equation (B11) is valid to linear order in the spin mixing conductance  $g_{\uparrow\downarrow i}$ , but for arbitrary spin accumulation  $u_{si\parallel}$ , magnon chemical potential  $u_{mi}$ , and electron and magnon temperatures  $u_{eQi}$  and  $u_{mQi}$ . Expanding Eq. (B11) to lowest order in the differences  $u_{si\parallel} - u_{mi}$  and  $u_{eQi} - u_{mQi}$  and taking the limit  $\hbar\omega_0/k_B T \rightarrow 0$  gives Eq. (33) of the main text [34, 52].

To obtain the nonlinear response relation (101), we expand Eq. (B11) to second order in the potential differences. Again taking the limit  $\hbar\omega_0/k_B T \rightarrow 0$ , we find

that the response matrices in Eq. (101) read

$$\mathcal{A}_{si} = \frac{3k_T^3 \text{Re } g_{\uparrow\downarrow i}}{4\pi^{3/2} s \zeta(3/2)} \begin{pmatrix} 2\zeta(1/2) & -2\zeta(3/2) \\ -6\zeta(3/2) & -15\zeta(5/2) \end{pmatrix} \mathcal{N}, \quad (\text{B12})$$

$$\mathcal{A}_{Qi} = \frac{3k_T^3 \text{Re } g_{\uparrow\downarrow i}}{8\pi^{3/2} s \zeta(3/2)} \begin{pmatrix} 12\zeta(3/2) & 30\zeta(5/2) \\ 50\zeta(5/2) & 175\zeta(7/2) \end{pmatrix} \mathcal{N}, \quad (\text{B13})$$

$$\mathcal{B}_s = \frac{2}{\zeta(3/2)} \mathcal{N} \begin{pmatrix} 4\zeta(1/2) & 6\zeta(3/2) \\ 6\zeta(3/2) & 15\zeta(5/2) \end{pmatrix} \mathcal{N}, \quad (\text{B14})$$

$$\mathcal{B}_Q = -\frac{5}{\zeta(3/2)} \mathcal{N} \begin{pmatrix} 4\zeta(3/2) & 10\zeta(5/2) \\ 10\zeta(5/2) & 35\zeta(7/2) \end{pmatrix} \mathcal{N}, \quad (\text{B15})$$

where we abbreviated

$$\mathcal{N} = \begin{pmatrix} 4\zeta(3/2) & 10\zeta(3/2) \\ 10\zeta(3/2) & 35\zeta(5/2) \end{pmatrix}^{-1}. \quad (\text{B16})$$

The spin current source  $\delta i_{si}$  of Eq. (101) may then be conveniently expressed as

$$\begin{aligned} \delta i_{si\parallel}(\Omega) = & \frac{1}{i_{\text{FN}i}} |\mathbf{m}_{\text{eq}} \cdot \mathbf{e}_y|^2 \sum_{j,k} \int \frac{d\omega}{2\pi} \theta_{\text{SH}j} \theta_{\text{SH}k} \sigma_{\text{N}j} \sigma_{\text{N}k} E_j(\omega_+) E_k(\omega_-)^* \\ & \times \left[ (-Z_{\text{Ni}} [\delta_{ij} - \zeta_{ij\parallel}(\omega_+)] \Phi_{ij}(\omega_+) Z_{\text{N}j}) \mathcal{A}_{si} \begin{pmatrix} \zeta_{ik\parallel}(\omega_-) \\ \phi_{ik}(\omega_-) \end{pmatrix} + (\zeta_{ij\parallel}(\omega_+) \Phi_{ij}(\omega_+)) \mathcal{B}_s \begin{pmatrix} \zeta_{ik\parallel}(\omega_-) \\ \phi_{ik}(\omega_-) \end{pmatrix} \right], \end{aligned} \quad (\text{B17})$$

where  $i_{\text{FN}i}$ , which has the dimension of “charge current density” was defined in Eq. (102) and the dimensionless coefficients  $\zeta_{ij\parallel}(\omega)$ ,  $\Phi_{ij}(\omega)$ , and  $\phi_{ij}(\omega)$  were defined in Eqs. (65), (73), and (74), respectively. The heat current source  $\delta i_{Qi}$  takes the same form as Eq. (B17) under

exchange of indices  $s \leftrightarrow Q$ .

### Bilinear STD response

A similar expression for the source terms corresponding to the precession of the magnetization  $\delta i_{si\parallel}$ ,  $\delta i_{Qi}$ , and  $\delta i_{si\perp}$  of Eq. (112) reads

$$\begin{aligned} \begin{pmatrix} \delta i_{si\parallel}(\Omega) \\ \delta i_{Qi}(\Omega) \end{pmatrix} = & \frac{1}{2\pi i_{\text{F}}} |\mathbf{e}_{\perp} \cdot \mathbf{e}_y|^2 \sum_{j,k} \int d\omega E_j(\omega_+) E_k(\omega_-)^* \theta_{\text{SH}j} \theta_{\text{SH}k} \sigma_{\text{N}j} \sigma_{\text{N}k} (-1)^{j-1} \\ & \times \left[ (-1)^{i+k} [\eta_{ij\perp}(\omega_+) (1 - \zeta_{ik\perp}(\omega_-)^*) + \eta_{ij\perp}(-\omega_+)^* (1 - \zeta_{ik\perp}(-\omega_-))] Z_{\text{Ni}} \mathcal{Z}_{\text{FN}i}^{-1} \begin{pmatrix} 1 \\ 0 \end{pmatrix} \right. \\ & \left. - [\eta_{ij\perp}(\omega_+) \zeta_{ik\perp}(\omega_-)^* + \eta_{ij\perp}(-\omega_+)^* \zeta_{ik\perp}(-\omega_-)] \begin{pmatrix} 1 \\ 0 \end{pmatrix} \right], \end{aligned} \quad (\text{B18})$$

$$\begin{aligned} \delta i_{si\perp}(\Omega) = & -\frac{1}{2\pi i_{\text{F}}} (\mathbf{e}_{\perp}^* \cdot \mathbf{e}_y) (\mathbf{m}_{\text{eq}} \cdot \mathbf{e}_y) \sum_{j,k} \int d\omega E_j(\omega_+) E_k(\omega_-)^* \theta_{\text{SH}j} \theta_{\text{SH}k} \sigma_{\text{N}j} \sigma_{\text{N}k} (-1)^{j-1} \\ & \times [(-1)^{i+k} Z_{\text{Ni}} \mathcal{Z}_{\text{FN}i\perp}^{-1} \eta_{ij\perp}(\omega_+) (1 - \zeta_{ik\parallel}(\omega_-)^*) + \eta_{ij\perp}(\omega_+) \zeta_{ik\parallel}(\omega_-)^*], \end{aligned} \quad (\text{B19})$$

where  $i_{\text{F}}$  is defined in Eq. (72).

- 
- [1] K. Uchida, J. Xiao, H. Adachi, J. Ohe, S. Takahashi, J. Ieda, T. Ota, Y. Kajiwara, H. Umezawa, H. Kawai, G. E. W. Bauer, S. Maekawa, and E. Saitoh, *Nat. Mater.* **9**, 894 (2010).
  - [2] G. E. W. Bauer, E. Saitoh, and B. J. van Wees, *Nat. Mater.* **11**, 391 (2012).
  - [3] M. I. Dyakonov and V. I. Perel, *JETP Lett.* **13**, 467 (1971).
  - [4] J. E. Hirsch, *Phys. Rev. Lett.* **83**, 1834 (1999).
  - [5] C. O. Avci, A. Quindeau, C.-F. Pai, M. Mann, L. Caretta, A. S. Tang, M. C. Onbasli, C. A. Ross, and G. S. D. Beach, *Nat. Mater.* **16**, 309 (2017).
  - [6] M. Yang, L. Sun, Y. Zeng, J. Cheng, K. He, X. Yang, Z. Wang, L. Yu, H. Niu, T. Ji, G. Chen, B. Miao, X. Wang, and H. Ding, *Nat. Commun.* **15**, 3201 (2024).
  - [7] M. Weiler, M. Althammer, F. D. Czeschka, H. Huebl, M. S. Wagner, M. Opel, I.-M. Imort, G. Reiss, A. Thomas, R. Gross, and S. T. B. Goennenwein, *Phys. Rev. Lett.* **108**, 106602 (2012).
  - [8] S. Y. Huang, X. Fan, D. Qu, Y. P. Chen, W. G. Wang, J. Wu, T. Y. Chen, J. Q. Xiao, and C. L. Chien, *Phys. Rev. Lett.* **109**, 107204 (2012).
  - [9] H. Nakayama, M. Althammer, Y.-T. Chen, K. Uchida, Y. Kajiwara, D. Kikuchi, T. Ohtani, S. Geprags, M. Opel, S. Takahashi, R. Gross, G. E. W. Bauer, S. T. B. Goennenwein, and E. Saitoh, *Phys. Rev. Lett.* **110**, 206601 (2013).
  - [10] C. Hahn, G. de Loubens, O. Klein, M. Viret, V. V. Naleto, and J. Ben Youssef, *Phys. Rev. B* **87**, 174417 (2013).
  - [11] N. Vlietstra, J. Shan, V. Castel, J. Youssef, G. E. W. Bauer, G. E. W. Bauer, and V. Wees, *Applied Physics Letters* **103**, 032401 (2013).
  - [12] M. Althammer, S. Meyer, H. Nakayama, M. Schreier, S. Altmannshofer, M. Weiler, H. Huebl, S. Geprags, M. Opel, R. Gross, D. Meier, C. Klewe, T. Kuschel, J.-M. Schmalhorst, G. Reiss, L. Shen, A. Gupta, Y.-T. Chen, G. E. W. Bauer, E. Saitoh, and S. T. B. Goennenwein, *Phys. Rev. B* **87**, 224401 (2013).
  - [13] J. Lotze, H. Huebl, R. Gross, and S. T. B. Goennenwein, *Phys. Rev. B* **90**, 174419 (2014).
  - [14] J.-G. Choi, J. W. Lee, and B.-G. Park, *Phys. Rev. B* **96** (2017), 10.1103/physrevb.96.174412.
  - [15] Y.-T. Chen, S. Takahashi, H. Nakayama, M. Althammer, S. T. B. Goennenwein, E. Saitoh, and G. E. W. Bauer, *Phys. Rev. B* **87**, 144411 (2013).
  - [16] Y.-T. Chen, S. Takahashi, H. Nakayama, M. Althammer, S. T. B. Goennenwein, E. Saitoh, and G. E. W. Bauer, *J. Phys. Condens. Matter* **28**, 103004 (2016).
  - [17] X.-P. Zhang, F. S. Bergeret, and V. N. Golovach, *Nano Lett.* **19**, 6330 (2019).
  - [18] S. S.-L. Zhang and S. Zhang, *Phys. Rev. Lett.* **109**, 096603 (2012).
  - [19] S. S.-L. Zhang and S. Zhang, *Phys. Rev. B* **86**, 214424 (2012).
  - [20] Y. Kajiwara, K. Harii, S. Takahashi, J. Ohe, K. Uchida, M. Mizuguchi, H. Umezawa, H. Kawai, K. Ando, K. Takanashi, S. Maekawa, and E. Saitoh, *Nature* **464**, 262 (2010).
  - [21] L. J. Cornelissen, J. Liu, R. A. Duine, J. B. Youssef, and B. J. van Wees, *Nat. Phys.* **11**, 1022 (2015).
  - [22] S. T. B. Goennenwein, R. Schlitz, M. Pernpeintner, K. Ganzhorn, M. Althammer, R. Gross, and H. Huebl, *Appl. Phys. Lett.* **107**, 172405 (2015).
  - [23] R. Schlitz, S. Velez, A. Kamra, C.-H. Lambert, M. Lamme, S. T. B. Goennenwein, and P. Gambardella, *Phys. Rev. Lett.* **126**, 257201 (2021).
  - [24] J. Li, Y. Xu, M. Aldosary, C. Tang, Z. Lin, S. Zhang, R. Lake, and J. Shi, *Nat. Commun.* **7**, 10858 (2016).
  - [25] H. Wu, C. H. Wan, X. Zhang, Z. H. Yuan, Q. T. Zhang, J. Y. Qin, H. X. Wei, X. F. Han, and S. Zhang, *Phys. Rev. B* **93**, 060403(R) (2016).
  - [26] P. Muduli, R. Schlitz, T. Kosub, R. Hubner, A. Erbe, D. Makarov, and S. T. B. Goennenwein, *APL Mater.* **9**, 021122 (2020).
  - [27] L. Berger, *Phys. Rev. B* **54**, 9353 (1996).
  - [28] J. C. Slonczewski, *J. Magn. Magn. Mater.* **159**, L1 (1996).
  - [29] Y. Tserkovnyak, A. Brataas, and G. E. W. Bauer, *Phys. Rev. Lett.* **88**, 117601 (2002).
  - [30] A. Brataas, Y. V. Nazarov, and G. E. W. Bauer, *Phys. Rev. Lett.* **84**, 2481 (2000).
  - [31] J. Xiao, G. E. W. Bauer, K. Uchida, E. Saitoh, and S. Maekawa, *Phys. Rev. B* **81**, 214418 (2010).
  - [32] S. A. Bender and Y. Tserkovnyak, *Phys. Rev. B* **91**, 140402(R) (2015).
  - [33] H. Adachi, K.-I. Uchida, E. Saitoh, and S. Maekawa, *Rep. Prog. Phys.* **76**, 036501 (2013).
  - [34] L. Cornelissen, K. Peters, R. Duine, G. Bauer, and B. Wees, *Phys. Rev. B* **94**, 014412 (2016).
  - [35] R. Schmidt and P. W. Brouwer, *Phys. Rev. B* **103** (2021), 10.1103/physrevb.103.014412.
  - [36] J. A. Fulop, S. Tzortzakis, and T. Kampfrath, *Adv. Opt. Mater.* **8**, 1900681 (2020).
  - [37] J. Walowski and M. Munzenberg, *J. Appl. Phys.* **120**, 140901 (2016).
  - [38] C. O. Avci, K. Garello, A. Ghosh, M. Gabureac, S. F. Alvarado, and P. Gambardella, *Nat. Phys.* **11**, 570 (2015).
  - [39] C. O. Avci, J. Mendil, G. S. D. Beach, and P. Gambardella, *Phys. Rev. Lett.* **121**, 087207 (2018).
  - [40] G. Liu, X.-G. Wang, Z. Z. Luan, L. F. Zhou, S. Y. Xia, B. Yang, Y. Z. Tian, G.-H. Guo, J. Du, and D. Wu, *Phys. Rev. Lett.* **127**, 207206 (2021).
  - [41] A. A. Tulapurkar, Y. Suzuki, A. Fukushima, H. Kubota, H. Maehara, K. Tsunekawa, D. D. Jayaprawira, N. Watanabe, and S. Yuasa, *Nature* **438**, 339 (2005).
  - [42] J. C. Sankey, P. M. Braganca, A. G. F. Garcia, I. N. Krivorotov, R. A. Buhrman, and D. C. Ralph, *Phys. Rev. Lett.* **96**, 227601 (2006).
  - [43] L. Liu, T. Moriyama, D. C. Ralph, and R. A. Buhrman, *Phys. Rev. Lett.* **106**, 036601 (2011).
  - [44] K. Kondou, H. Sukegawa, S. Mitani, K. Tsukagoshi, and S. Kasai, *Appl. Phys. Express* **5**, 073002 (2012).
  - [45] A. Ganguly, K. Kondou, H. Sukegawa, S. Mitani, S. Kasai, Y. Niimi, Y. Otani, and A. Barman, *Applied Physics Letters* **104**, 072405 (2014).
  - [46] M. Schreier, T. Chiba, A. Niedermayr, J. Lotze, H. Huebl, S. Geprags, S. Takahashi, G. E. W. Bauer, R. Gross, and S. T. B. Goennenwein, *Phys. Rev. B* **92**, 144411 (2015).
  - [47] J. Sklenar, W. Zhang, M. B. Jungfleisch, W. Jiang, H. Chang, J. E. Pearson, M. Wu, J. B. Ketterson, and

- A. Hoffmann, *Phys. Rev. B* **92**, 174406 (2015).
- [48] T. Chiba, G. E. W. Bauer, and S. Takahashi, *Phys. Rev. Applied* **2**, 034003 (2014).
- [49] S. S.-L. Zhang and G. Vignale, *Phys. Rev. B* **94**, 140411 (2016).
- [50] X.-G. Wang, Z.-W. Zhou, Y.-Z. Nie, Q.-L. Xia, and G.-H. Guo, *Phys. Rev. B* **97** (2018), 10.1103/physrevb.97.094401.
- [51] W. P. Sterk, D. Peerlings, and R. A. Duine, *Phys. Rev. B* **99** (2019), 10.1103/PhysRevB.99.064438.
- [52] D. A. Reiss, T. Kampfrath, and P. W. Brouwer, *Phys. Rev. B* **104** (2021), 10.1103/physrevb.104.024415.
- [53] A. J. Schellekens, K. C. Kuiper, R. R. J. C. de Wit, and B. Koopmans, *Nat. Commun.* **5**, 4333 (2014).
- [54] I. Razdolski, A. Alekhin, N. Ilin, J. P. Meyburg, V. Rodatis, D. Diesing, U. Bovensiepen, and A. Melnikov, *Nat. Commun.* **8**, 15007 (2017).
- [55] J. Kimling, G.-M. Choi, J. T. Brangham, T. Matalla-Wagner, T. Huebner, T. Kuschel, F. Yang, and D. G. Cahill, *Phys. Rev. Lett.* **118**, 057201 (2017).
- [56] T. S. Seifert, S. Jaiswal, J. Barker, S. T. Weber, I. Razdolski, J. Cramer, O. Gueckstock, S. F. Maehrlein, L. Nadvornik, S. Watanabe, C. Ciccarelli, A. Melnikov, G. Jakob, M. Münzenberg, S. T. B. Goennenwein, G. Woltersdorf, B. Rethfeld, P. W. Brouwer, M. Wolf, M. Kläui, and T. Kampfrath, *Nat. Commun.* **9**, 2899 (2018).
- [57] T. Kampfrath, M. Battiato, P. Maldonado, G. Eilers, J. Nötzold, S. Mährlein, V. Zbarsky, F. Freimuth, Y. Mokrousov, S. Blügel, M. Wolf, I. Radu, P. M. Oppeneer, and M. Münzenberg, *Nat. Nanotechnol.* **8**, 256 (2013).
- [58] T. S. Seifert, N. M. Tran, O. Gueckstock, S. M. Rouze-gar, L. Nadvornik, S. Jaiswal, G. Jakob, V. V. Temnov, M. Münzenberg, M. Wolf, M. Kläui, and T. Kampfrath, *J. Phys. D Appl. Phys.* **51**, 364003 (2018).
- [59] V. Sluka, *Phys. Rev. B* **96**, 214412 (2017).
- [60] O. Johansen, H. Skarsvåg, and A. Brataas, *Phys. Rev. B* **97**, 054423 (2018).
- [61] O. Franke, “Python script to evaluate main results of this article,” <https://zenodo.org/doi/10.5281/zenodo.13348735> (2024), accessed: 2024-8-20.
- [62] J. Flipse, F. K. Dejene, D. Wagenaar, G. E. W. Bauer, J. Ben Youssef, and B. J. van Wees, *Phys. Rev. Lett.* **113**, 027601 (2014).
- [63] L. J. Cornelissen, J. Shan, and B. J. van Wees, *Phys. Rev. B* **94** (2016), 10.1103/PhysRevB.94.180402.
- [64] J. S. Jamison, Z. Yang, B. L. Giles, J. T. Brangham, G. Wu, P. C. Hammel, F. Yang, and R. C. Myers, *Phys. Rev. B* **100** (2019), 10.1103/physrevb.100.134402.
- [65] M. I. Dyakonov and V. I. Perel, *Phys. Lett. A* **35**, 459 (1971).
- [66] S. Takahashi, H. Imamura, and S. Maekawa, in *Concepts in Spin Electronics*, edited by S. Maekawa (Oxford University Press, 2006) pp. 343–370.
- [67] Y. Tserkovnyak, A. Brataas, and G. E. W. Bauer, *Phys. Rev. B* **66**, 224403 (2002).
- [68] Z. Qiu, K. Ando, K. Uchida, Y. Kajiwara, R. Takahashi, H. Nakayama, T. An, Y. Fujikawa, and E. Saitoh, *Appl. Phys. Lett.* **103**, 092404 (2013).
- [69] M. Weiler, M. Althammer, M. Schreier, J. Lotze, M. Pernpeintner, S. Meyer, H. Huebl, R. Gross, A. Kamra, J. Xiao, Y.-T. Chen, H. Jiao, G. E. W. Bauer, and S. T. B. Goennenwein, *Phys. Rev. Lett.* **111**, 176601 (2013).
- [70] V. Cherepanov, I. Kolokolov, and V. L’vov, *Phys. Rep.* **229**, 81 (1993).
- [71] Z. Shi, Q. Xi, J. Li, Y. Li, M. Aldosary, Y. Xu, J. Zhou, S.-M. Zhou, and J. Shi, *Phys. Rev. Lett.* **127**, 277203 (2021).
- [72] C. W. Corti, *Platin. Met. Rev.* **28**, 164 (1984).
- [73] J. R. Rumble, T. J. Bruno, and M. J. Doa, eds., *CRC Handbook of Chemistry and Physics*, 103rd ed., CRC Handbook of Chemistry and Physics (CRC Press, Boca Raton, FL, 2022).
- [74] S. R. Boona and J. P. Heremans, *Phys. Rev. B* **90** (2014), 10.1103/PhysRevB.90.064421.
- [75] A. A. Tulapurkar and Y. Suzuki, *Phys. Rev. B* **83**, 012401 (2011).
- [76] T. Taniguchi, *Appl. Phys. Express* **9**, 073005 (2016).
- [77] D. A. Reiss and P. W. Brouwer, *Phys. Rev. B* **106**, 144423 (2022).
- [78] F. Guimarães, M. dos Santos Dias, J. Bouaziz, A. M. de Almeida Costa, R. Muniz, and S. Lounis, *Sci. Rep.* **7**, 3686 (2017).
- [79] B. Han, B. Wang, Z. Yan, T. Wang, D. Yang, X. Fan, Y. Wang, and J. Cao, *Phys. Rev. Appl.* **13**, 014065 (2020).
- [80] Y. Cheng, J. Tang, J. J. Michel, S. K. Chong, F. Yang, R. Cheng, and K. L. Wang, *Phys. Rev. Lett.* **130**, 086703 (2023).
- [81] M. Althammer, *Phys. Status Solidi Rapid Res. Lett.* **15**, 2100130 (2021).
- [82] L. J. Cornelissen, J. Liu, B. J. van Wees, and R. A. Duine, *Phys. Rev. Lett.* **120** (2018), 10.1103/physrevlett.120.097702.
- [83] S. Shim, M. Mehraeen, J. Sklenar, J. Oh, J. Gibbons, H. Saglam, A. Hoffmann, S. S.-L. Zhang, and N. Mason, *Phys. Rev. X* **12**, 021069 (2022).
- [84] Z. Zheng, Y. Gu, Z. Zhang, X. Zhang, T. Zhao, H. Li, L. Ren, L. Jia, R. Xiao, H.-A. Zhou, Q. Zhang, S. Shi, Y. Zhang, C. Zhao, L. Shen, W. Zhao, and J. Chen, *Nano Lett.* **23**, 6378 (2023).
- [85] B. Wang, Q. Zhang, Y. Guo, W. Li, B. Zhang, and J. Cao, *J. Appl. Phys.* **135** (2024), 10.1063/5.0186776.
- [86] Y. Lv, J. Kally, D. Zhang, J. S. Lee, M. Jamali, N. Samarth, and J.-P. Wang, *Nat. Commun.* **9**, 111 (2018).
- [87] M. Mehraeen, P. Shen, and S. S.-L. Zhang, *Phys. Rev. B* **108**, 014411 (2023).
- [88] S. E. Sullivan, H. Lee, A. Weathers, and L. Shi, *Phys. Rev. B* **107**, L140412 (2023).
- [89] S. Daimon, R. Iguchi, T. Hioki, E. Saitoh, and K.-I. Uchida, *Nat. Commun.* **7**, 13754 (2016).
- [90] G. Chiriacò and A. J. Millis, *Phys. Rev. B* **102** (2020), 10.1103/physrevb.102.085116.
- [91] S. M. Rezende and J. C. López Ortiz, *Phys. Rev. B* **91**, 104416 (2015).
- [92] N. P. Padture and P. G. Klemens, *J. Am. Ceram. Soc.* **80**, 1018 (2005).
- [93] M. Schreier, A. Kamra, M. Weiler, J. Xiao, G. E. W. Bauer, R. Gross, and S. T. B. Goennenwein, *Phys. Rev. B* **88**, 094410 (2013).